Meteorol Atmos Phys (2014) 123:115–141
DOI 10.1007/s00703-013-0290-4

ORIGINAL PAPER

A study on the structure and precipitation of Morakot (2009) induced by the Central Mountain Range of Taiwan

Yi-Chih Huang · Yuh-Lang Lin

Received: 20 October 2012 / Accepted: 5 October 2013 / Published online: 26 October 2013

Abstract The three-dimensional structures and ingredients leading to extremely heavy precipitation associated with the passage of Typhoon Morakot (2009) over the Central Mountain Range (CMR) of Taiwan are investigated. Using a numerical model, the track, track deflection, characteristic rainbands, and precipitation patterns and maxima are successfully reproduced after verification against observational data. The high-level outward flow of the secondary circulation around the eyewall is not very clear even during Morakot's strongest stage. In the control case, the eyewall collapses within 5 h after landfall that is closely associated with limited precipitation along the track after landfall. During the early stage of landfall, the deep convection on the windward (west) side of the CMR helps strengthening the secondary circulation. A quantitative comparison of total precipitable water, translation speed, and orographic lifting among 12 typhoons in recent years causing large accumulated rainfall in Taiwan shows that the abundant water vapor around Taiwan outweighs translation speed and orographic lifting in resulting in the record-breaking precipitation. It is found that the major processes leading to strong upward motion in the extremely heavy precipitation during 0000 UTC 8 August–0000 UTC 9 August are initiated by orographic lifting by CMR.

Responsible editor: M. Kaplan.

Y.-C. Huang (✉) · Y.-L. Lin
Department of Energy and Environmental Systems,
North Carolina A&T State University, Greensboro, NC, USA
e-mail: dscpln@gmail.com

Present Address:
Y.-C. Huang
ARC-ENV, Center for Advanced Information Science
and Technology, University of Aizu, Tsuruga, Ikki-machi,
Aizuwakamatsu, Fukushima 965-8580, Japan

Y.-L. Lin
Department of Physics, North Carolina A&T State University,
Greensboro, NC, USA

1 Introduction

Typhoon Morakot (2009) resulted in disasters such as landslide, mudslide, flash flood, etc. and many casualties in the calamity. Before it made landfall, Morakot belongs to category 1 on the Saffir–Simpson hurricane scale (Simpson 1974), however, the rainfall of Morakot on 8 August alone exceeds 1,500 mm is astonishing. Although there have been many investigations about Morakot, yet there is no numerical study with thorough verifications of track, intensity, vertical maximum radar reflectivity, and accumulated precipitation with observational analysis made in meteorological centers. In this study, by conducting relatively accurate numerical simulations, we focus on the investigation of the three-dimensional structural change in the vicinity of Morakot's center and the factors leading to the extremely heavy precipitation. To determine the dominant factors, which make Morakot so unique, we compare total precipitable water, translation speed, and orographic lifting of Morakot with those in 11 other typhoons.

There are few papers investigate the three-dimensional (3D) structural change of Morakot except, for example, Nguyen and Chen (2011) and Lin et al. (2011). Nguyen and Chen (2011) discuss the wind field structures with different initializations of the simulations of Morakot. Unfortunately, their simulated tracks and precipitation patterns are very different from observations. Lin et al. (2011) discuss the rainbands over the Taiwan Strait. Unfortunately, their simulated precipitation is far less than that observed. For

example, the accumulated precipitation associated with Morakot at the Alishan station is about 3000 mm in the observed accumulated precipitation analysis in several publications (e.g., Liang et al. 2011; Huang et al. 2011), and the webpages of Central Weather Bureau, whereas it is less 2,000 mm during 6 August–10 August in UTC in both observation and simulation in Lin et al. (2011). The poor simulations in the above research indicate the difficulties of simulations of Morakot. When the simulated track and precipitation patterns are significantly different from observations, the structure of Morakot is not realistic and keeps changing with time due to orographic effects. Hence, the time evolution of 3D structure of Morakot, especially on the eyewall and secondary circulation, has yet to examine, and thus, is one of the topics this study would like to address.

Generally speaking, there would be heavy rainfall close to the track of a typhoon. However, there was limited precipitation close to the track of Morakot after landfall. Originally, the convective activity close to Morakot's center develops well. The asymmetric rainfall patterns in Taiwan could be associated with the change of the three-dimensional structure of Morakot after landfall. Some studies demonstrate the impacts of land or orography on the development of a tropical cyclone. The orographically induced decreases of latent and kinetic energy cause a tropical cyclone filled quickly (Bender et al. 1985). Principally, the reduction of evaporation is responsible for tropical disturbance failing to develop on land (Tuleya 1994). Asymmetric structure could stem from quasi-discontinuity of surface heating and latent heating in idealized simulations (Chen and Yau 2003). Orographic influence could lead to decoupling between Doppler velocities and reflectivity (Lee et al. 2000). The asymmetric orographic forcing leads to the asymmetric precipitation patterns of Typhoon Nari (2001) after landfall (Yang et al. 2011). However, in the case of Morakot, the composite reflectivity exists to the south of the typhoon center before it made landfall due to the convergence of Morakot's circulation and the prevailing southwesterly flow. The special characteristics of Morakot such as precipitation analysis, satellite cloud analysis and radar reflectivity analysis can be found in Jou et al. (2010), Wang et al. (2010), and Wu et al. (2011). When Morakot was in the ocean stage, there were deep convections close to the eyewall. It is unusual that there is limited precipitation around the track of a typhoon after landfall. This study will use accurate numerical simulations to examine where the asymmetric precipitation patterns stem from, especially why there was limited precipitation around the track of Morakot after landfall.

The common ingredients leading to extremely heavy rainfall related to orography have been used to point out that high precipitation efficiency, a low-level jet, steep orography, favorable mountain geography and a confluent flow, strong synoptically forced upward vertical motion, a moist unstable low-level flow, a high moist flow upstream, a large, preexisting convective system, and slow movement of the convective system may lead to heavy orographic precipitation (Lin 2007). In the case of Morakot, several ingredients have been proposed to be responsible for the extremely heavy precipitation, such as the monsoonal influence on precipitation patterns, terrain lifting effects, slow moving of Morakot, and moisture supply corresponding to monsoon surges (Hong et al. 2010; Chien and Kuo 2011; Wu et al. 2011). In terms of water vapor, it is suggested that abundant water vapor was supplied by the southwesterly flow inserted in multiscale large-scale circulation (Hong et al. 2010) and strengthened by monsoon gyre (Ge et al. 2010). In addition, extra water vapor transported from Typhoon Goni (2009) could be significant (Xu et al. 2011). With regard to the slow translation after Morakot made the landfall, it is proposed that the coalescence of Morakot first with the quasi-biweekly oscillation and then with the Madden-Julian oscillation intensified large-scale southwesterly flow, resulting in turning the track northward and moving very slowly, and thus producing extremely heavy rainfall in southern Taiwan (Wu et al. 2011). In addition, it is shown that the strong northerly wind between Morakot and the anticyclone to the west weakened the northward steering flow associated with low-frequency oscillation (Liang et al. 2011). The maximum accumulated precipitation is reduced dramatically in the simulation with near-doubled translation speed based on EnKF data assimilation although the rainfall patterns in the control run are different from those in observation (Yen et al. 2011).

In a composite study of 19 tropical storms, it is demonstrated that the rainfall associated with the passage of a typhoon was proportional to the reciprocal of the translation speed (Chien and Kuo, 2011), which is consistent with the ingredient equation of precipitation in Doswell et al. (1996), Lin et al. (2001a, b), and Lin (2007). Furthermore, convergence and orographic lifting are emphasized in the mesoscale processes leading to the extremely heavy precipitation (Lin et al. 2011). The importance of orographic lifting in extremely heavy rainfall has also been pointed out by Hong et al. (2010), Ge et al. (2010), Chien and Kuo (2011), and Wu et al. (2011). Apparently, abundant water vapor, slow translation, and orographic lifting have the contribution to the extremely heavy precipitation associated with Morakot. However, quantitatively, the relative importance of abundant water vapor, slow translation, and orographic lifting is still unclear. In this study, these three factors are compared quantitatively among Morakot and other 11 typhoons to determine which factor(s) play the most significant role in producing the heavy orographic precipitation associated with Morakot.

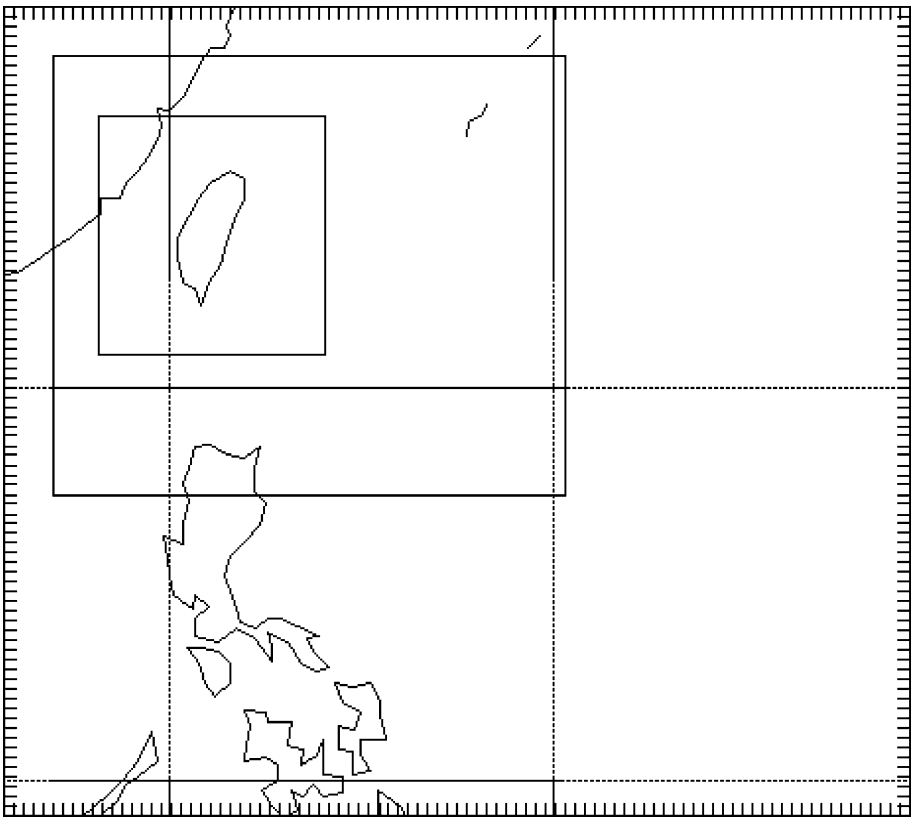

Fig. 1 The three nested domains used for numerical simulations of this study

Although there are a number of studies already done on Morakot, yet there is no numerical research having successful verification of track, intensity, vertical maximum radar reflectivity, and accumulated precipitation by comparing with those in meteorological centers. Thus, there is a need to conduct successful numerical modeling to understand the time evolution of 3D structure close to Morakot's center, the interaction of Morakot's outer circulation and its synoptic environment, and the quantitatively major factors responsible for the extremely heavy precipitation. Numerical simulation is a good tool in revealing the detail of a typhoon. Because the intensity of Morakot is only category 1 on the Saffir–Simpson hurricane scale and there are limited data over Western Pacific Ocean, it is difficult to conduct a good simulation even only in terms of the asymmetric rainfall patterns associated with Morakot (Wu et al. 2010). In this study, we employ the Advanced Research WRF (Weather Research and Forecasting) model (ARW) Model (Skamarock et al. 2008) to conduct numerical simulations, which are verified in Sect. 3. After the verification, it would be convincible to examine time evolution of the 3D structure of Morakot, asymmetric precipitation patterns, and the effects of the terrain on precipitation. Additionally, the study applies NOAA storm relative 16 km microwave-based total precipitable water imagery to the analysis of water vapor.

The paper is organized as follows. In Sect. 2, the ARW model, experiment design, radar reflectivity data, the total precipitable water data and best track data will be described. The verifications of simulated results will be performed in Sect. 3. The analysis on the time evolution of the 3D structure is conducted in Sect. 4. The analysis of several factors causing extremely heavy precipitation, including upward motion, water vapor and slow translation speed, will be given in Sect. 5. A summary can be found in Sect. 6.

2 Model description, experiment design and data

The ARW is employed to simulate the development of Morakot in the study. As found in other modeling studies, results simulated by limited-area numerical models are sensitive to domain size, mainly due to imperfect lateral boundary conditions. After some tests, the two-way triple-nested grid (27, 9, 3 km) is applied to this study as shown in Fig. 1. Vertically, there are 28 stretched σ levels for all the nested domains with the top at about 50 hPa and a higher resolution in the planetary boundary layer. The time intervals are 150, 50, and 16.7 s, respectively. The simulations of triple-nested grid in the study start with 0000 UTC 3 August 2009 and end at 0000 UTC 10 August 2009.

The physics options used in the simulations include Goddard microphysics scheme (Tao et al. 1989), Kain-Fritsch cumulus scheme (Kain 2004), Rapid Radiative

Table 1 The settings for all numerical experiments and their associated averaged Froude numbers on 8 August

Experiments	Conditions	U* (m/s)	H* (m)	Fr
CTL	The control case	28	3,223	0.87
NT	Terrain elevation set to 0	34	0	∞
OC	Land is replaced by ocean	41	0	∞

* The wind speed is the mean upstream wind speed on 8 August. The terrain elevation is from CTL with 3-km resolution

Transfer Model longwave radiation physics scheme (Mlawer et al. 1997), Dudhia shortwave radiation scheme (Dudhia 1989), and Yonsei University scheme of planetary boundary layer (Hong et al. 2006). When grid interval is <10 km, whether the cumulus parameterization scheme should be included in physics options is still under debating in the meteorology community. In the study, the cumulus parameterization scheme is activated in all nested domains to avoid energy accumulation at grid points. NCEP Global Forecast System (GFS) 1° data are used as initial and boundary conditions. The NCEP daily, high-resolution, real-time, global, sea surface temperature (SST) analysis on a 0.5° grid (ftp://polar.ncep.noaa.gov/pub/history/sst/) is employed to update the SST during time integrations. There is no bogus vortex initialization applied to the GFS data.

In the study, we plan to explore the impacts of terrain on the structure of Morakot and the precipitation associated with the passage of the typhoon. In the sensitivity experiments, all the parameters are held the same as the control case (CTL) except the changes in the terrain elevation or land to ocean. The experiment of ocean replaces land over Taiwan with ocean (Table 1).

The radar composite reflectivity data are originally from the Central Weather Bureau of Taiwan. The total precipitable water imaginary data are combined by a mixing algorithm (Kidder and Jones 2007) from the three advanced microwave sounding units (AMSU) installed on NOAA satellites and five special sensor microwave imagers (SSMI) on the Department of Defense satellites (http://rammb.cira.colostate.edu/products/tc_realtime). The best track data from the web site http://agora.ex.nii.ac.jp/digital-typhoon/index.html.en are employed in verification and the discussion about the factors, resulting in extremely heavy precipitation in Sect. 5b.

3 Verification of simulations of the control case

The verification of the CTL simulation includes track, intensity, vertical maximum radar reflectivity, and accumulated precipitation. There are four radars in Taiwan, which provide vertical composite reflectivity within their ranges. Also, totally there are 404 surface weather observational and automatic stations in Taiwan, which include meteorological stations and automatically observed rainfall stations. The coverage of these stations is pretty complete in Taiwan except in the eastern mountainous regions. Hence, the vertical maximum radar reflectivity and the accumulated precipitation in the analysis of observational data are the objective standards to evaluate the performance of simulations in the control case. Note that the best tracks and intensity estimated by meteorological centers such as the Joint Typhoon Warning Center (JTWC), Japan Meteorological Agency (JMA), and Central Weather Bureau (CWB) are subjective products, mainly due to limited observational data over the ocean, which raised some concerns in best track and intensity inconsistencies in the past.

In the CTL, there are not many differences in the patterns of physical fields between the results in different resolutions. Quantitatively, the simulation of 9 km resolution (CTL-9) is the best in almost every aspect of track, intensity, maximum reflectivity, and accumulated precipitation except the maximum accumulated precipitation during 0000 LST 7 August–0000 LST 8 August with 897.1 mm (9 km resolution) and 1,068.6 mm (3 km resolution) compared with the observation 1,003.5 mm. Since the resolution of CTL-9 falls into the so-called no man's land in cumulus and microphysics parameterization schemes, we will focus on discussing the result of CTL-3 in verification and analysis.

3.1 Track and intensity

Environmental steering flow is a good measure for typhoon direction. Tropical cyclones move about 10°–20° to the left of the steering flow the in Northern hemisphere (Chan and Gray 1982). In the study, we calculate the steering flow by averaging the mass-weighted mean wind within a radius of 378 km (14 grid points) between 850 and 300 hPa from the CTL. The simulated track is close to the JMA best track after 1200 UTC 6 August. Thus, the environmental steering flow since 1200 UTC 6 August would be reliable. Morakot slowed down since 1200 UTC 6 August because of terrain blocking from the CMR. The steering flow decelerates and turns from southeasterly to southerly, then to southwesterly (Fig. 2a). Note that the southerly environmental steering flow before 0000 UTC 8 August is consistent with the merging large-scale circulations moving northward (Hong et al. 2010). After Morakot crosses CMR, both the environmental steering flow and the propagation speed of Morakot are <2 ms^{-1} because of the hindrance of the steep CMR (Fig. 2a). Then, the environmental steering changed from southerly to southwesterly, finally resulting in Morakot's moving to northeastward (Fig. 2a). Thus, we may

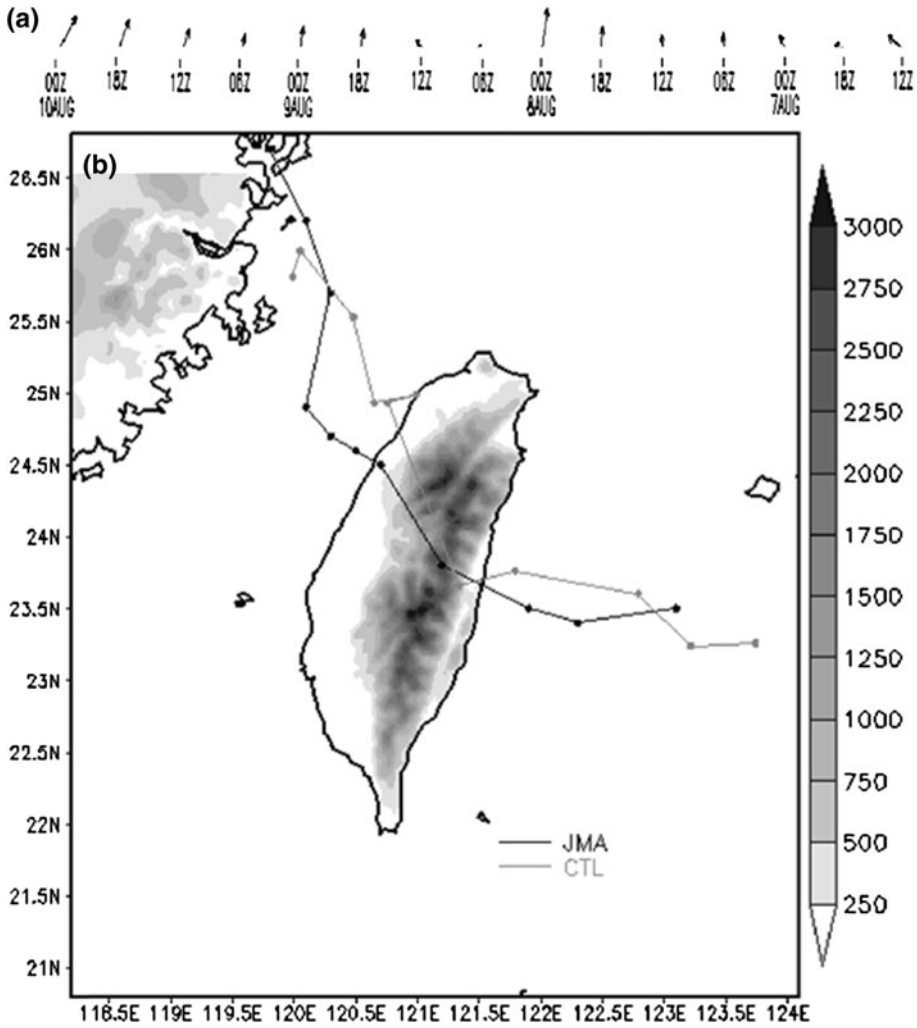

Fig. 2 **a** The environmental steering flow from CTL with 27 km resolution (CTL-27). **b** The JMA best track and the CTL track with 3-km resolution (CTL-3) every 3 h from 0000 7 August to 1200 UTC 9 August. The terrain elevations are *shaded* (in m)

conclude that Morakot's translation is dominated by its environmental steering flow.

The minimum sea level pressure from JTWC is much higher than those from JMA and CWB. We were unable to obtain maximum wind speed data online from CWB. Hence, we will compare the track and intensity in the simulation with those from JMA. Figure 2b displays the JMA best track and the CTL-3 during 0000 UTC 7 August–1800 UTC 9 August 2009. The average deviation is 74.64 km and the root mean square of deviation is 80.58 km. The simulated movements fall behind JMA best track before 0600 UTC 8 August 2009 and are pretty close to JMA best track since then until 1200 UTC 9 August 2009 (Fig. 2b). Comparing with the JMA maximum wind speed, in general, the intensity in the CTL-3 shows a slow spinup during the first 4 days and larger intensity than that of JMA data in the last 3 days (Fig. 3a, b). The largest simulated maximum wind speed (41 ms^{-1}) before the landfall is stronger than that of JMA (39 ms^{-1}). After the landfall, the trends of weakening intensity in JMA and the simulation are not much different from each other, and thus, the intensity in simulation is larger than that in JMA data on 8 and 9 August (Fig. 3). Simulated minimum sea level pressure demonstrates apparently stronger intensity than JMA data since 0000 UTC 7 August (Fig. 3b).

In summary, the simulation is able to capture the right track, especially on 8 and 9 August 2009, a critical period for producing extremely heavy rainfall, especially the slow translation during 0000 UTC 8 August–1200 UTC 8 August. This, in turn, produces the right rainfall patterns on subsection accumulated precipitation, albeit the drawbacks in overprediction of the intensity.

3.2 Composite reflectivity and accumulated precipitation

The comparison of the simulated composite reflectivity and observed radar reflectivity composite is shown in Fig. 4. The former including rain, snow, and graupel only accounts for the Rayleigh scattering range of drop sizes and assumes particles to be spheres of constant density and exponential distribution of size distribution. The intercept parameter for rain is

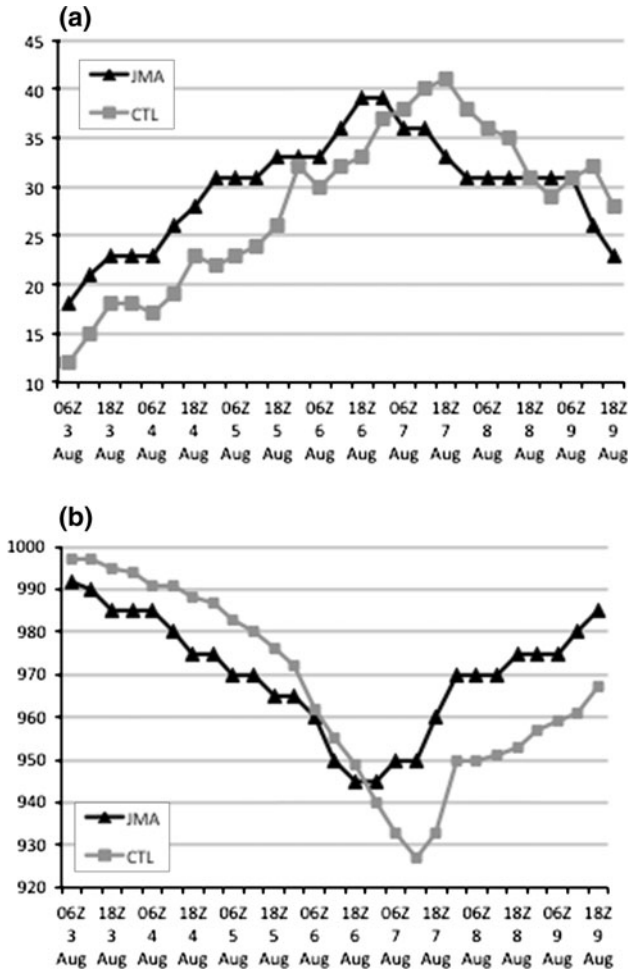

Fig. 3 **a** Maximum surface wind speed and **b** minimum sea level pressure from JMA analysis and the CTL-27 case. The simulated landfall time is at about 2200 UTC 7 August

constant (Reisner et al. 1998), whereas the intercept parameter for snow is a temperature-dependent value as described in Thompson et al. (2004). At 0000 UTC 8 August the center of Morakot is over the island of Taiwan. The major reflectivity pattern in observed radar reflectivity composite is located to the south of Morakot and extends toward east and northeast. Qualitative pattern of the simulated composite reflectivity is similar to that of the observation which has the strongest rain band to the south of Morakot's center, including the rain bands around CMR and the elongated rain band extending from the Taiwan Strait to CMR.

Furthermore, the observed rainfall data are analyzed based on Cressman objective analysis technique to compare the precipitation patterns and rainfall of the CTL cases in model simulations with the observational precipitation analysis. Figure 5 compares the simulated rainfall during 0000 LST 3 August–0000 LST 10 August 2009 where the LST (=UTC + 8 h) stands for local standard time. The simulated accumulated precipitation pattern captures that of the analysis of rain gauge data. In particular, the location of simulated maximum accumulated rainfall of the inner domain (CTL-3) is only <5.7 km away from the station with rainfall maximum in the observational data. Overall the simulated rainfall catches the observed patterns with higher rainfall. The maximum simulated rainfall is 3505 mm, which is about 22.9 % higher than the observed value. Due to strong variation with time, comparison of daily rainfall is more rigorous than that of the entire simulated period. Figure 6 is the comparison of daily rainfall on 7–9 August 2009 in local time. Basically, the daily rainfall patterns in observational data are well simulated. The elongated pattern of the simulated extremely heavy precipitation in southern Taiwan is much larger than the observational rainfall (Fig. 6b) and is orographically induced and originated from the strong wind associated with the simulated strong intensity of the typhoon. The simulated maximum accumulated rainfalls in these 3 days are 1,068.6, 1,931.2, and 1,385.7 mm, respectively, which are overpredicted about 6.5, 37.7, and 18.9 % more than the values in observational data, respectively.

The simulated total and daily rainfall patterns demonstrate excellent performance of the simulation in spite of the minor drawback in the overprediction of quantitative precipitation. The track in the simulation is then justified in illustrating the reasons, resulting in extremely heavy precipitation during the passage of Morakot over Taiwan.

4 Orographic and land effects on the 3D structure of Morakot (2009)

One major issue of this study is to investigate the orographic and land effects on the time evolution of the three-dimensional structure of Morakot. Especially, we would like to focus on the reflectivity, wind, and equivalent potential temperature (θ_e) fields in three stages: over the ocean, during landfall, and after landfall but moved to northern Taiwan. The largest reflectivity of Morakot over the ocean is to the south of the eye, while the minimum is to the north of the eye. The reflectivity to the east of the eye is almost the same as that to the west (Fig. 7). These reflectivity patterns do not change much until the Morakot's circulation is affected by the CMR (Fig. 9a). Because the CMR is so high and steep, the Morakot's circulation is strongly influenced and the transportation of water vapor is blocked, and thus the reflectivity to the west of the eye (lee side of the CMR) is no longer equal to that to the east (Fig. 9a) as well as orographically induced rain is pronounced since then. The diameter of the eye near the low boundary is about 0.78° width in longitude at 23.5°N (Fig. 7). The eye is less visible after landfall (Figs. 7, 9a). Within 2 h after landfall, the cloud-free eye disappeared.

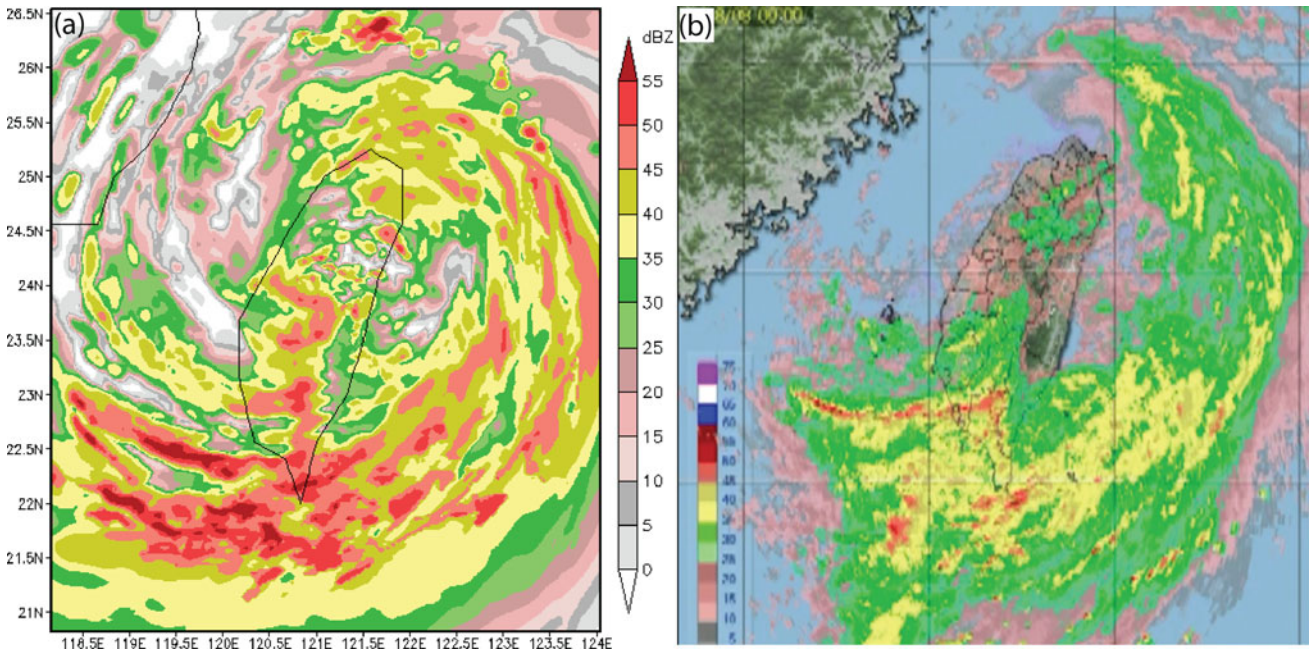

Fig. 4 **a** Composite reflectivity (dBZ) from case CTL-3 at 0000 UTC 8 August and **b** maximum radar reflectivity at 0000 UTC 8 August

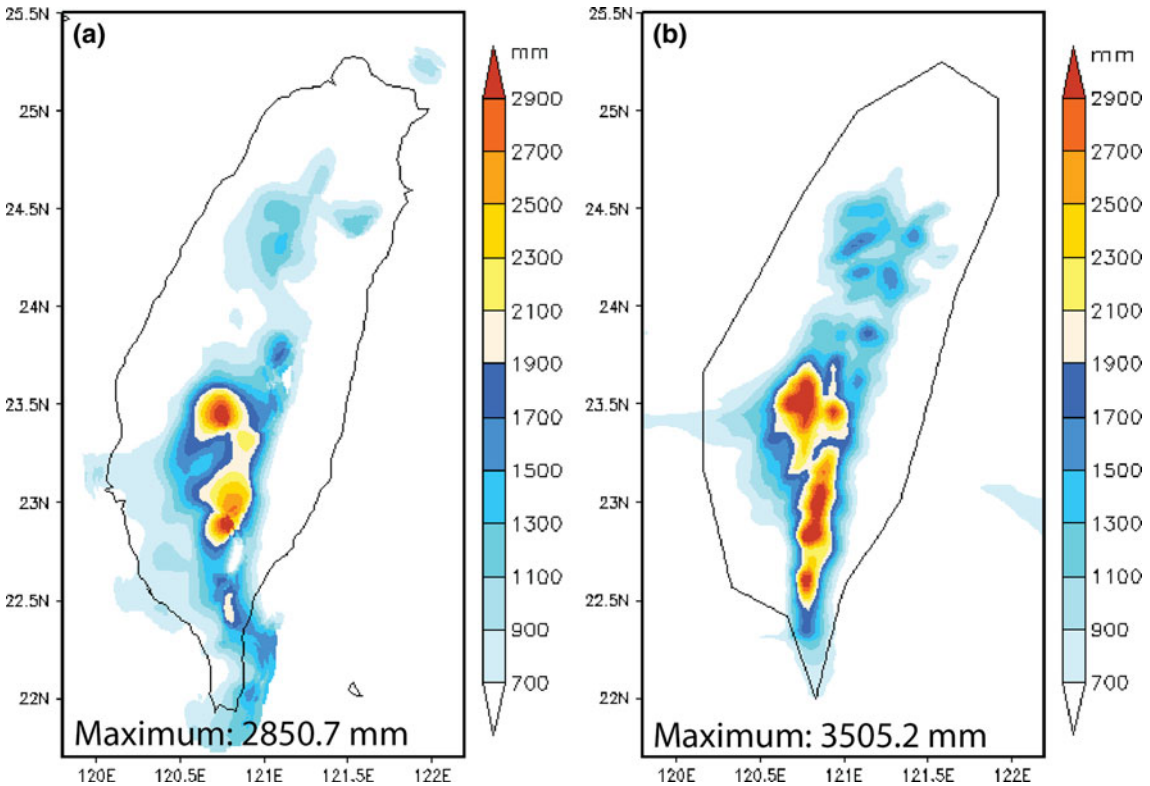

Fig. 5 The accumulation rainfall over Taiwan during 0000 LST (local standard time) 3 August–0000 LST 8 August from **a** observation and **b** case CTL-3

The longitude-height cross section of Morakot on 1200 UTC 7 August demonstrates some typical characteristics of a tropical cyclone as shown in Fig. 8. The largest wind speed is near the height of 1 km, the top of the marine boundary layer (MBL) (Fig. 8a). The radius of maximum wind (RMW) increases with height (Fig. 8a). The

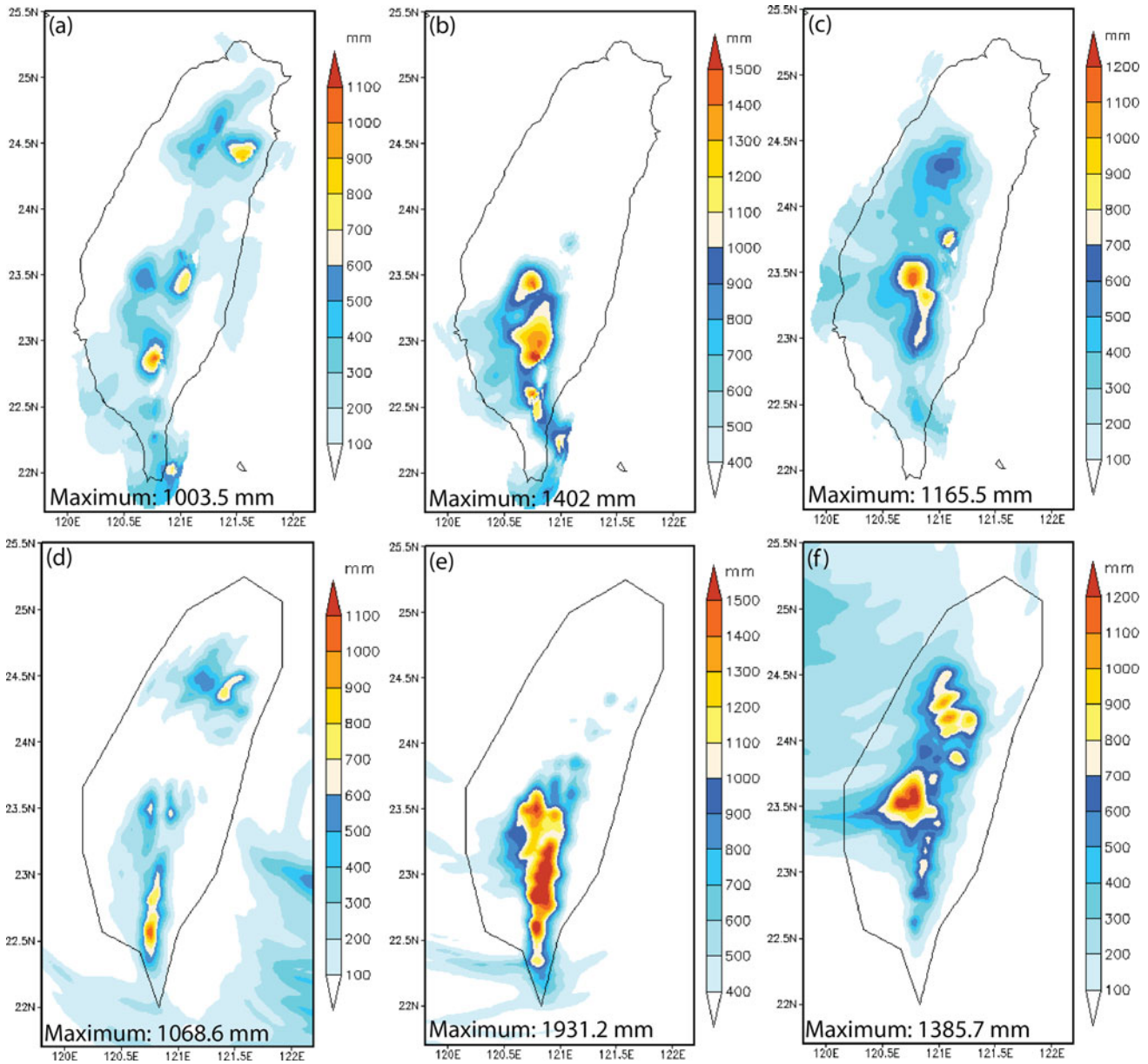

Fig. 6 The accumulation rainfall over Taiwan from (*upper*) observation and (*lower*) case CTL-3 during **a**, **d** 0000 LST 7 August–0000 LST 8 August, **b**, **e** 00 LST 8 August–0000 LST 9 August, and **c**, **f** 0000 LST 9 August–00 LST 1000 August

secondary circulation around the eyewall is only inward in low levels, and then upward at the eyewall, but the outward flow in high levels is not very clear (Fig. 8a). The maximum upward velocity is larger than 1.5 ms^{-1} located at about 1.5 km height, and the maximum downward velocity is larger than 0.5 ms^{-1} around the upward velocity (Fig. 8b). There is a wide region with low θ_e ($\theta_e < 365$ K) within the eye (Fig. 8b). This implies that the upward motion is not strong enough everywhere at the eyewall to prevent low θ_e air from going into the region within the eyewall. The minimum wind speed is at about 10.5 km height around the center of the eye (Fig. 8a). To the east, rain bands do not extend to the distance (Fig. 8b). In the eyewall, there is a large upward motion associated with deep convection; the upward motions elsewhere are rather weak (Fig. 8b). The large equivalent potential temperature ($\theta_e > 376$ K) is within the eyewall, whereas the lowest θ_e ($\theta_e < 352$ K) is at the sides about 1–4 km height (Fig. 8b).

During the landfall, Fig. 9 shows the differences in the wind and the composite reflectivity fields between the CTL case and the experiments of no terrain (NT) and no land (i.e., all ocean, OC) when the storm just made landfall. The distributions of large reflectivity (>25 dBZ) in NT and OC are different from those in CTL. Again, the orographic

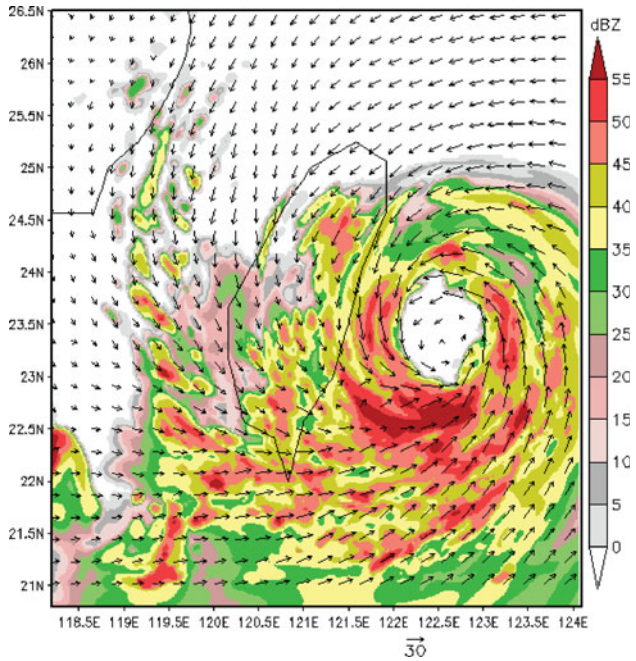

Fig. 7 The composite reflectivity and wind vectors on 1200 7 August simulated in case CTL-3

blocking effects in the CTL case are so significant that there is no reflectivity around the eyewall. Instead, the maxima are in the mountainous regions extending southward. Therefore, orographically induced rainfall and its associated reflectivity are very important in the CTL case. The reflectivity maxima in NT and OC remain around the southern part of the eyewall extending southward. In addition, the eye in the OC is much larger than that in the other two cases, which indicates the significance of ocean on the development of a typhoon.

The longitude-height cross section of Morakot simulated in the CTL case shows that the secondary circulation close to the shore behaves very different from that over the ocean, with the help of deep convection over the western slope of the CMR. Note that this deep convection at 121E is initiated by the orographic lifting. The maximum wind speed above the ocean is still near the MBL, and the one close to the shore is not very clear over the Taiwan Strait. The high-θ_e (>372 K) area in the eyewall close to the ocean is separated by moderate θ_e (370 K) air. The transport of moderate θ_e by the anticyclonic flow tends to separate low-θ_e air about 2.5 km height above the ocean (Fig. 10a). In NT, close to the shore the secondary circulation of the upward motion within the eye, and the outward flow in high levels is rather lucid, whereas there is no distinct secondary circulation over the ocean, which indicates slower collapse of eyewall than that in the CTL. The convections over land close to the eyewall help to form the secondary circulation; but the deep convections above ocean deflect inflow at lower levels (Fig. 10b). Also, at this stage, the storm has not yet developed very well in case OC. Hence, the secondary circulation is not clear because of the detracking deep convections and weak convections around eyewall. The high-θ_e area close to the lower boundary within the eye shows the impacts of high SST (Fig. 10c).

While Morakot moved to northern Taiwan, a comparison of the vertical structure between the CTL, NT, and OC cases on 0300 UTC 8 August is shown in Fig. 11. In CTL, there is no secondary circulation any more. The maximum wind speeds are still at about 1 km height. But the outward tilting RMW with height also no longer exists. The high-θ_e region (>371 K) is only limited to above 7 km, whereas the low-θ_e air (<364 K) is connected from one side to the other at about 5 km height (Fig. 11a). The above indicates that the eyewall has collapsed due to the destruction of Morakot's circulation by the steep and high CMR. In NT (Fig. 11b), the secondary circulation and outward tilting RMW with height are not as clear as in previous stages. The high-θ_e region (>371 K) extends to low levels in an irregular pattern. All the above indicate that the eyewall is decaying in both CTL and NT, and that ocean is important on sustaining the typhoon. In contrast, in case OC, the secondary circulation and outward tilting RMW with height to the west are obvious (Fig. 11c) because the storm is still developing due to the additional water vapor, latent heat and sensible heat from the lower boundary of ocean.

In this section, we demonstrated that the eye, eyewall, high-θ_e region within the eyewall, secondary circulation, and tilting RMW of Morakot are closely associated with the development of the storm, especially the deep convections around the eyewall. Over ocean the storm can develop continuously as in case OC. Hence, the secondary circulation is more obvious than that in the CTL case (Figs. 8a, 11c). Over land the eye, eyewall, high-θ_e region in the eyewall, secondary circulation, and tilting RMW of Morakot are decaying (Figs. 7, 8, 9, 10, 11), particularly those in the CTL case with high and steep terrain. Based on these experiments, the presence of land is much more substantial than terrain elevation for the development of Morakot. How do sensible heat, latent heat, and water vapor make impacts on the developments of Morakot is an important issue to be further investigated.

5 Factors leading to extremely heavy precipitation

The extremely heavy precipitation was mainly resulted from the convergence produced by Morakot's outer circulation and the southwesterly flow, orographic lifting, and instabilities. Special attention is paid to a region with a diameter at least 0.5° in the vicinity of the Morakot's

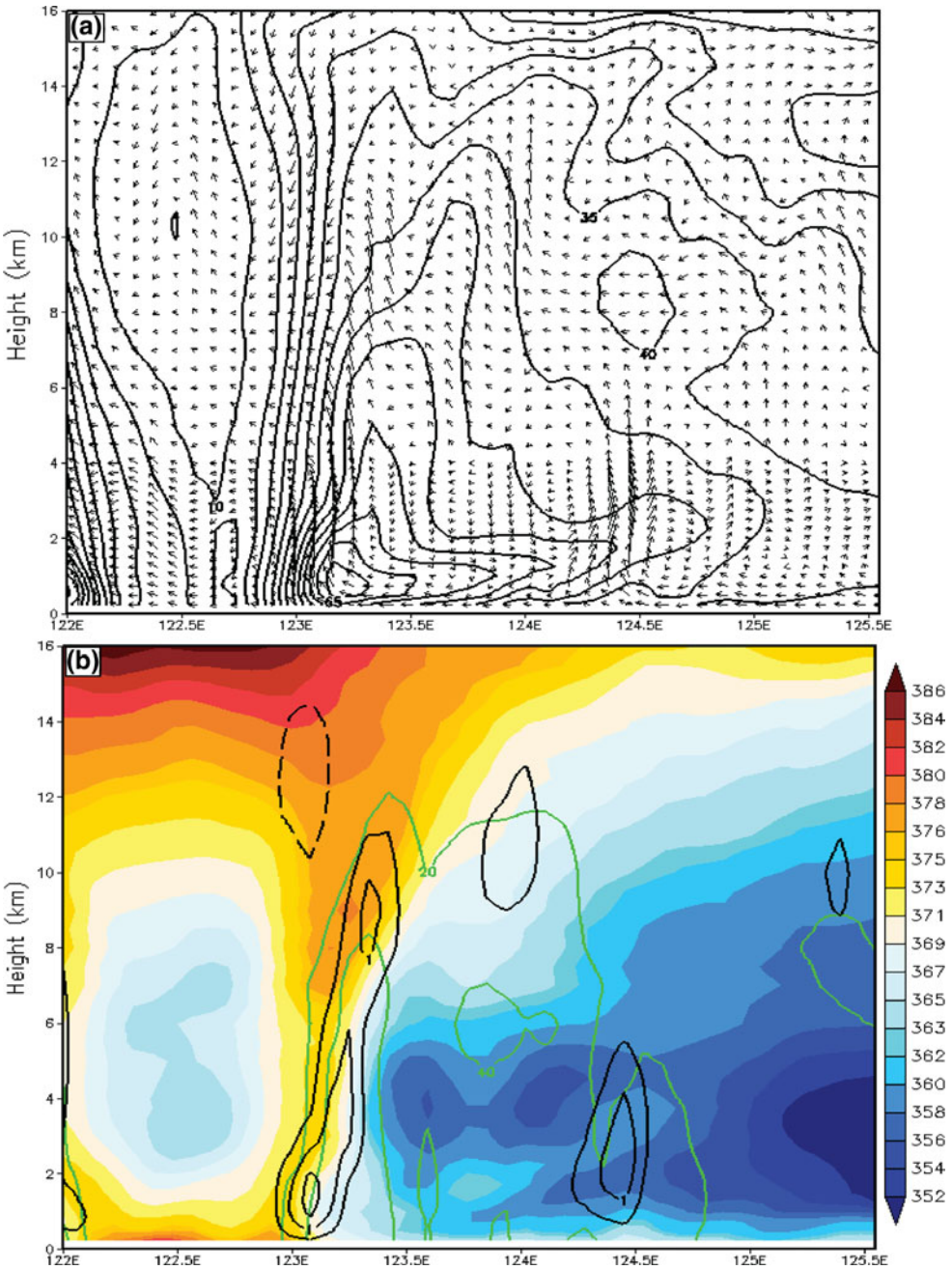

Fig. 8 The longitude-height cross section at 23.55°N of **a** the wind vectors and wind speed contours with interval 5 ms^{-1} and **b** the equivalent potential temperature (K) (*shaded*), composite reflectivity (*green*), and vertical velocity (*black*) with interval 0.5 ms^{-1} of Morakot on 1200 UTC 7 August simulated in the CTL-9 case

center, where the wind speed, convergence, and upward motion are much weaker, and less humid than those to the south of Morakot's center where orographic lifting and convergence between Morakot's circulation and the southwesterly monsoonal flow occurred (Figs. 11a, 12a–d) and produced heavy rainfall. Near the Morakot's center, it is relatively dry because of the blocking of the CMR on water vapor transportation (Fig. 9a) and the advection of very dry air to the east of the CMR due to adiabatic warming (Fig. 12a–c). The weak wind speed, convergence, and upward motion as well as low relative humidity close to Morakot's center are consistent with the collapse of Morakot's eyewall within 5 h (Figs. 10a, 11a). Away from Morakot's center to the south the strong wind, high humidity and convergence of Morakot's outer circulation and the southwesterly monsoonal flow help to lead to orographic lifting to produce extremely heavy precipitation (Figs. 12, 13). This is the main reason why the rainfall distribution was quite asymmetric and heavy precipitation mostly happened in southern Taiwan when Morakot was passing over northern Taiwan. The regions with strong flow convergence and orographic lifting moved northward accordingly as Morakot moved northward, and thus, led to heavy precipitation in northern Taiwan on 9 August

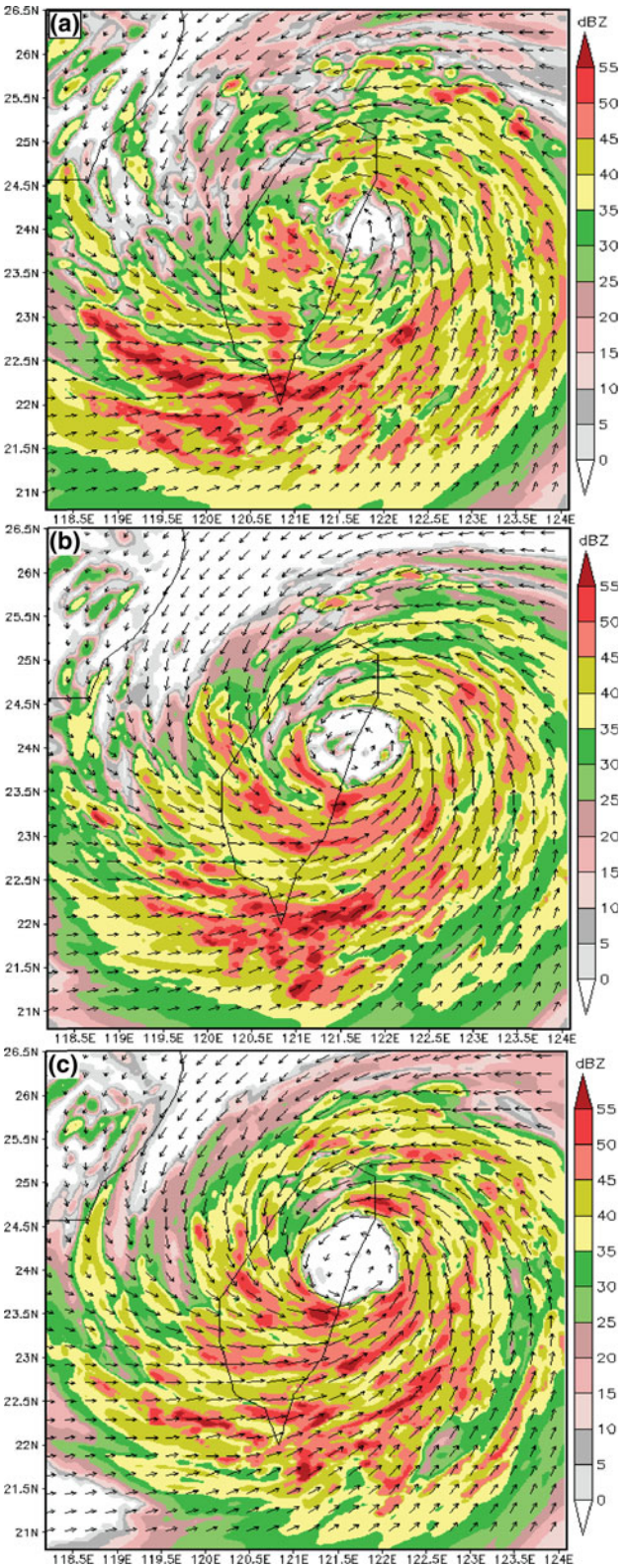

Fig. 9 The composite reflectivity (dBZ) at the time of landfall on **a** 2200 UTC 7 August simulated in the CTL-3 case, **b** 2000 UTC 7 August in no terrain (NT) case, and **c** 2200 UTC 7 August in ocean (OC) case. The time is chosen when Morakot's center just make landfall

(Fig. 12e, f). The much drier southwesterly flow associated with the initial (GFS) data could be the reason why the accumulated precipitation in the CTL case underpredicts the precipitation as Morakot moved away from Taiwan during 0000 UTC 9 August–0000 UTC 10 August (Fig. 12c–f). Of interest is the very dry regions to the east of the CMR caused by adiabatic warming associated with strong downslope wind (Fig. 12a–f).

5.1 Major processes leading to strong upward motion on August 8

Several processes can generate strong upward motion such as orographic lifting, convergence, and instabilities. Instability here includes moist absolute instability, conditional instability, and potential instability. In this study, we would like to identify the major processes leading to strong upward motion, especially for 0000–2400 UTC 8 August during which there is 1,503.5 mm rainfall observed at the station located at (23.51°N, 120.81°E). Therefore, we inspect the nearest vertical cross sections at (23.50°N, 120.76°E) in the CTL-3 having a maximum precipitation of 1970.8 mm and at (23.53°N, 120.59°E) in NT with precipitation of 785.1 mm during the period. The major process will be inferred by analyzing the simulated data causing extremely heavy rainfall in cases CTL and NT.

Concerning the orographic lifting, the low-level upward motion associated with flow over mountain may come from orography or environment, thus the vertical velocity can be divided and expressed as in Eq. (1), similar to that proposed in the ingredient approach of orographic rain (Lin et al. 2001a, b Lin 2007). However, frequently w_{oro} and w_{env} cannot be separated completely due to nonlinear interactions. To do so, w_{oro} is calculated by subtracting the vertical velocity in the case NT from that of case CTL as shown below in Eq. (2).

$$w = w_{oro} + w_{env} = V_H \cdot \nabla h + w_{env} \quad (1)$$

$$w_{oro} = w - w_{env} = w_{CTL} - w_{NT} \quad (2)$$

Because the vertical velocity in the case NT is so much smaller than that in case CTL, the orographically induced vertical velocity fields (Fig. 13) are reasonable despite the fact that the tracks in the CTL and NT cases are not exactly the same. The elongated region of strong upward motion is overpredicted, as discussed in the model verification in Sect. 3. Nevertheless, still the orographically induced vertical motion plays an important role in leading to extremely heavy precipitation on 8 August.

The positive values (shaded regions with warm colors) of environmental lapse rate minus moist adiabatic lapse rate and the very high relative humidity (>98 %, the region within contours) (Fig. 14a) along with the skew T plots

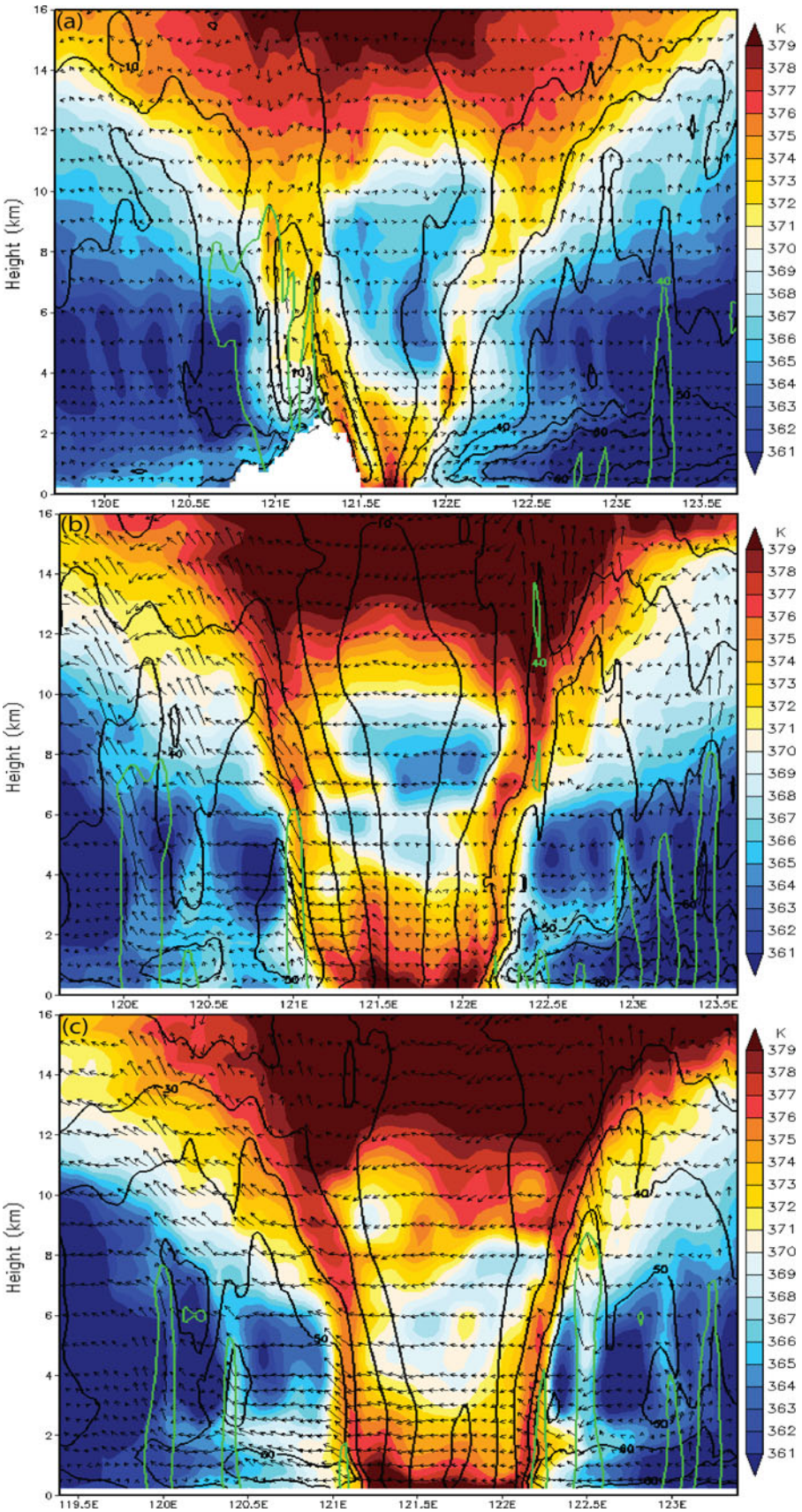

Fig. 10 The longitude-height cross section of the wind vectors and wind speed contours (*black*) with interval 5 ms^{-1}, the equivalent potential temperature (*shaded*), and composite reflectivity (40 dBZ) (*green*) of Morakot on **a** 2200 UTC 7 August at 23.92°N simulated in case CTL-3, and 2000 UTC 7 August simulated **b** case NT at 24.08°N and **c** case OC at 23.97°N

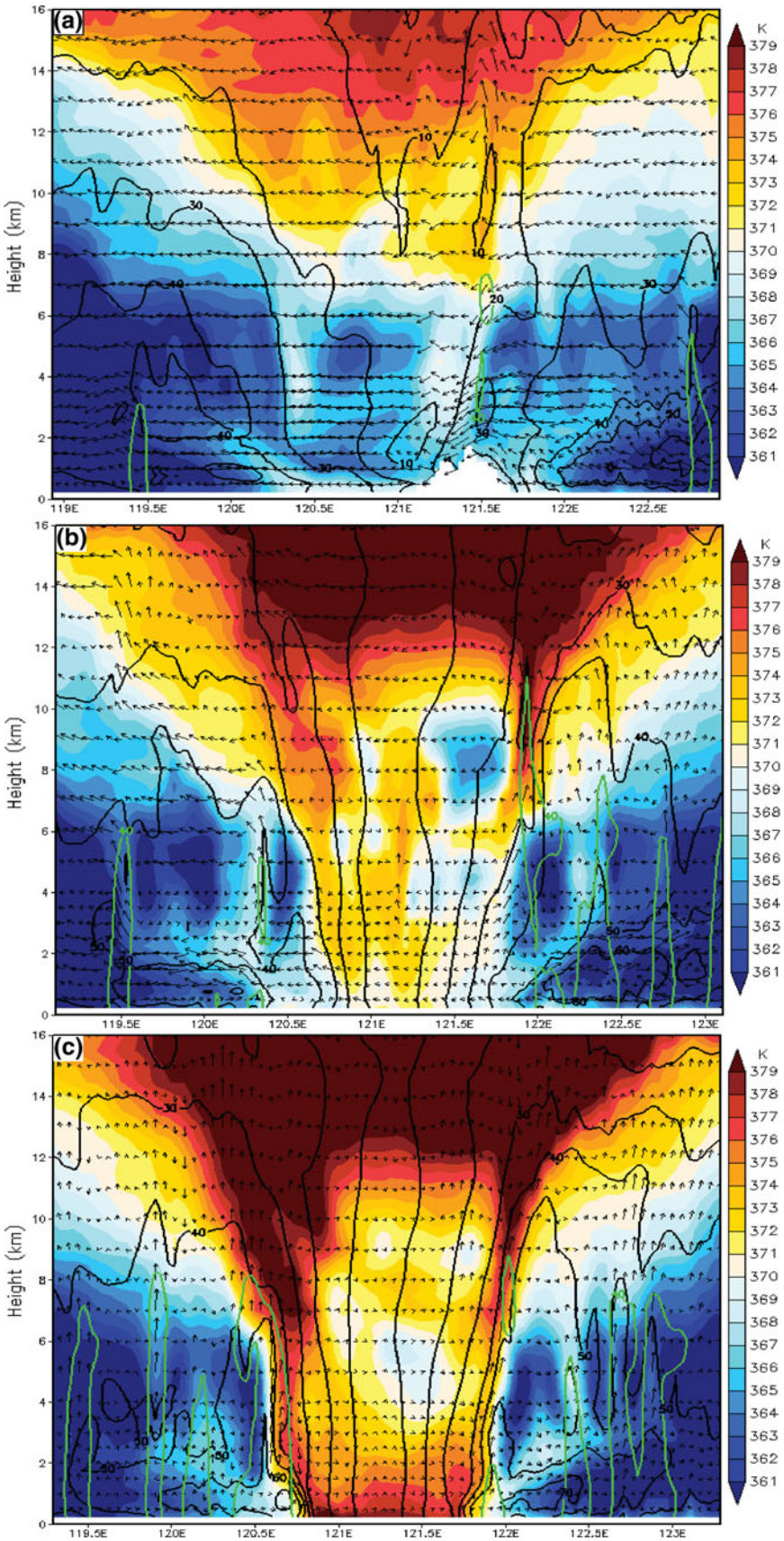

Fig. 11 The longitude-height cross section of the wind vectors and wind speed contours (*black*) with interval 5 ms^{-1}, the equivalent potential temperature (*shaded*), and composite reflectivity (40 dBZ) (*green*) of Morakot on 0300 UTC 8 August simulated in **a** case CTL-3 at 24.73 N, **b** case NT at 24.39 N and **c** case OC at 24.21 N

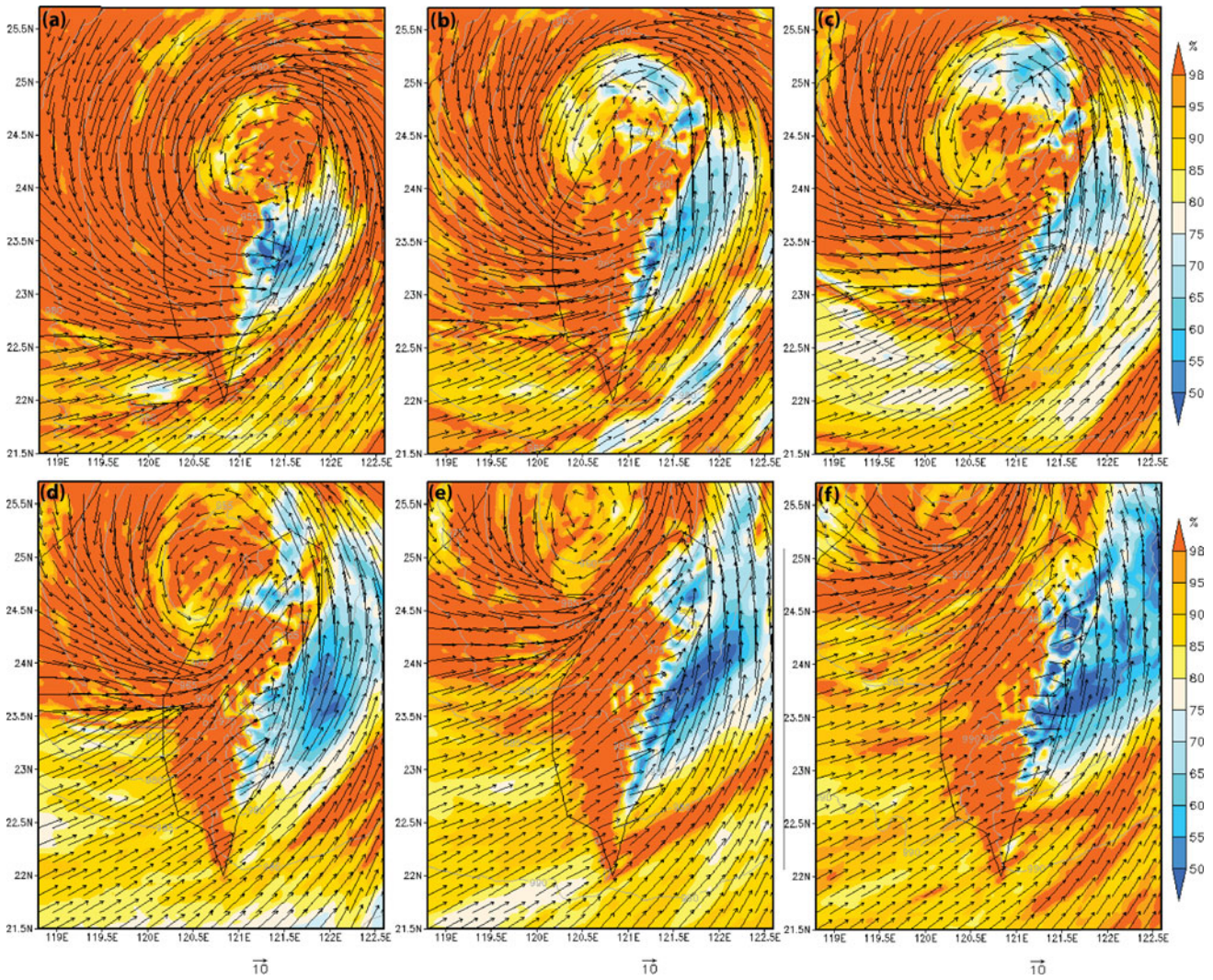

Fig. 12 Simulated relative humidity (*shaded*), and horizontal wind vector at **a** 0000 UTC 8 August, **b** 0600 UTC 8 August, **c** 1200 UTC 8 August, **d** 1800 UTC 8 August, **e** 0000 UTC 9 August, and **f** 0600 UTC 9 August from case CTL-3

(Fig. 15a) during 0900 UTC 6 August–0000 UTC 10 August indicate that moist absolute instability (MAI) could occur (Lin 2007) and help to produce heavy precipitation during the period. In fact, the MAI could occur in 9 August although the convective available potential energy (CAPE) is much smaller than that during the previous period. The negative vertical gradient of saturated equivalent potential temperature ($\partial\theta_e^*/\partial z$) (below shaded regions in dark blue colors above surface) along with high relative humidity (>98 %) indicates that conditional instabilities could occur on 7 August (Fig. 16a). The lifting condensation levels (LCLs) are generally low except during the period of 0300–1200 UTC 8 August. When the strong wind associated with the approaching Morakot occurred during 7–9 August, conditional instability could be triggered. In addition, the negative vertical gradients of equivalent potential temperature ($\partial\theta_e/\partial z$) (below shaded regions in dark blue colors above surface) along with high relative humidity (>98 %) indicate that conditional instabilities could occur from 7 August to early 8 August (Fig. 17a). The strong wind during 7–8 August is able to lift the full layer of atmosphere ahead of the mountain thus triggering the potential instability. Hence, instabilities, including moist absolute instability, conditional instability, and potential instability, appeared to be able to generate strong upward motion which can help to lead to heavy precipitation during 7–9 August at (23.50°N, 120.76°E).

Likewise, the processes leading to the strong upward motion in producing the maximum precipitation 785.1 mm at (23.53°N, 120.59°E) in case NT include convergence and instabilities. In this study, we would like to take a further investigation on instabilities on 8 August on both cases CTL and NT. The negative vertical gradients of θ_e and θ_e^* at the low levels are much smaller, if any, because

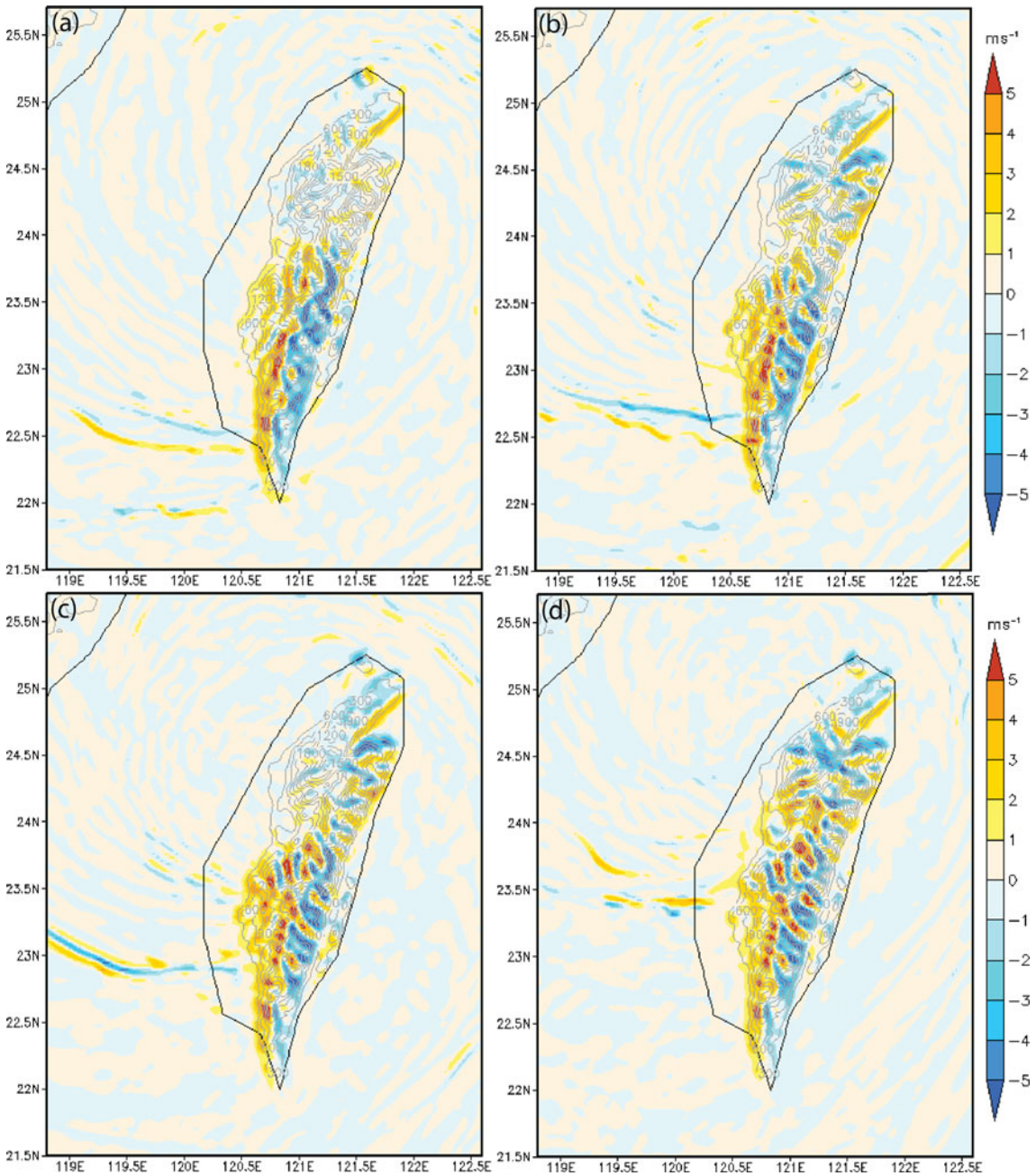

Fig. 13 Orographically induced vertical specific humidity flux (ms^{-1}) at **a** 0000, **b** 0600, **c** 1200, and **d** 1800 UTC 8 August in case CTL-3. *Gray lines* are topography contours

of strong vertical motion as well as much higher LCL on 8 August than any other days during 0000 UTC 3 August and 0000 UTC 10 August (Figs. 16, 17). In fact, the vertical gradients of θ_e and θ_e^* at the low levels are either neutral or stable near the surface most of time on 8 August (Figs. 16, 17). The CAPE is only 203, 128, 15, and 33 J kg^{-1} in the CTL case, as well as 216, 0, 2, and 31 J kg^{-1} in the case NT at 0000, 0600, 1200, and 1800 UTC 8 August, respectively (Fig. 15c, d). The above indicates that all these three instabilities are almost negligible for producing the upward motion in producing the extremely heavy rainfall during 0000 UTC 8–0000 UTC 9 August in both cases CTL and NT. Therefore, the maximum precipitation 785.1 mm in the case NT appears to be roughly initiated by horizontal convergence; the maximum precipitation 1,970.8 mm in the CTL can be roughly initiated by horizontal convergence and orographic lifting. The estimated precipitation initiated by orographic lifting is the difference between 1,970.8 mm and 785.1 mm without large error. Convergence appears

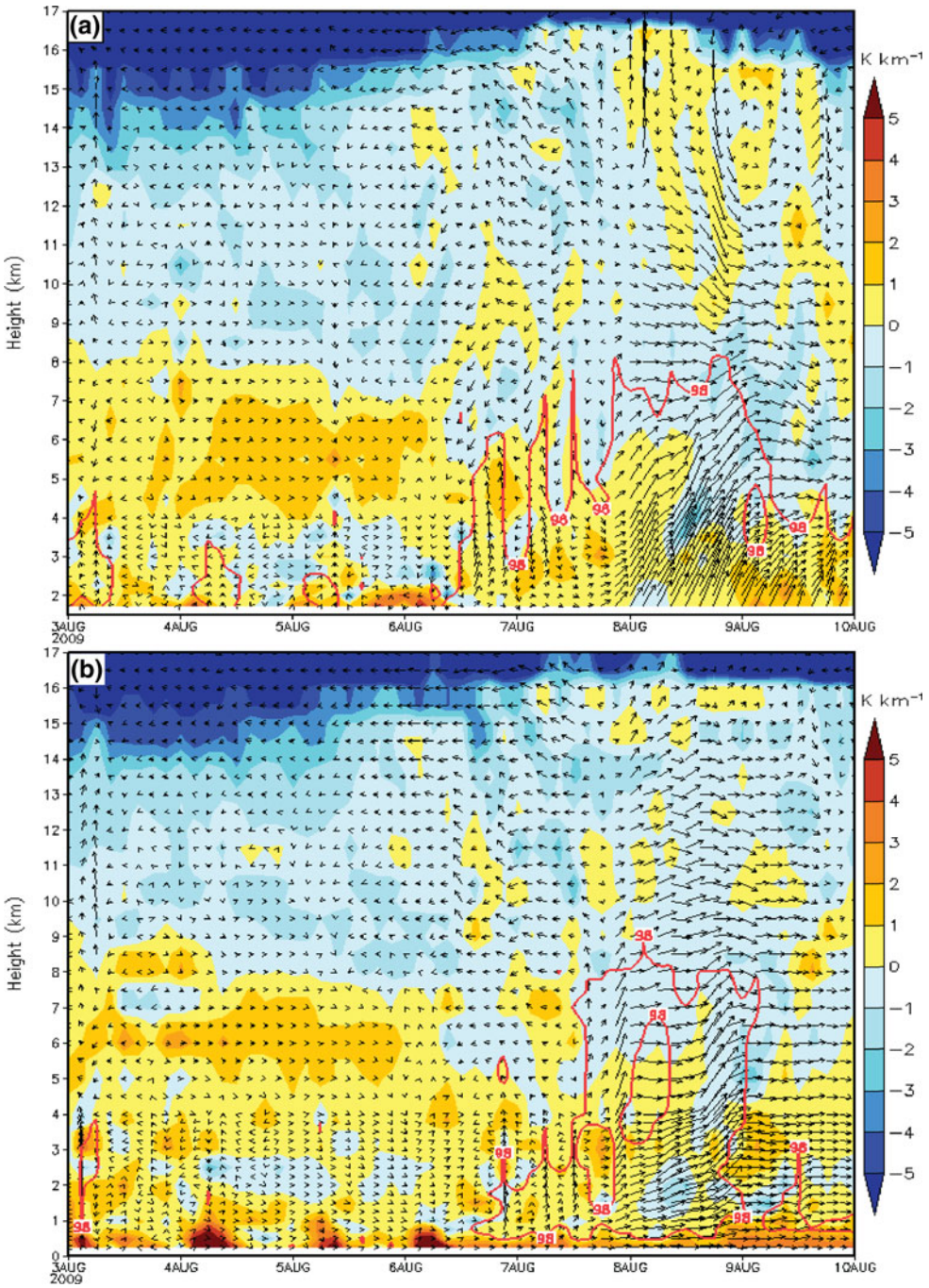

Fig. 14 The time-height cross section of the environmental lapse rate minus moist adiabatic lapse rate (K km^{-1}) simulated in **a** the CTL-3 case at (23.50°N, 120.76°E) and **b** the NT case at (23.53°N, 120.59°E). *Red lines* are 98 % relative humidity

to be outweighed by orographic lifting in the initiation processes leading to the strong upward motion in the extremely heavy precipitation. And thus, orographic lifting is the most viable dominant process in initiating the upward motion, resulting in the observed 1,503.5 mm rainfall at the station at (23.51°N, 120.81°E) during 0000 UTC 8 August–0000 UTC 9 August among other processes such as convergence between Morakot's circulation and the southwesterly flow, and instabilities although the exact simulated rainfall does not match well with the observed rainfall. As for 6–7 August the three instabilities cannot be ignored for generating the upward motion which help to produce the heavy precipitation because of very humid air in the low levels, much larger environmental lapse rate minus moist adiabatic lapse rate, θ_e and θ_e^*, much lower LCL, and much larger CAPE than those on 8 August (Figs. 14, 15, 16, 17). The orographic lifting and/or convergence could not be able to outrank instabilities for the upward motion producing the rainfall before 8 August. Hence, before 8 August, it is uncertain about the

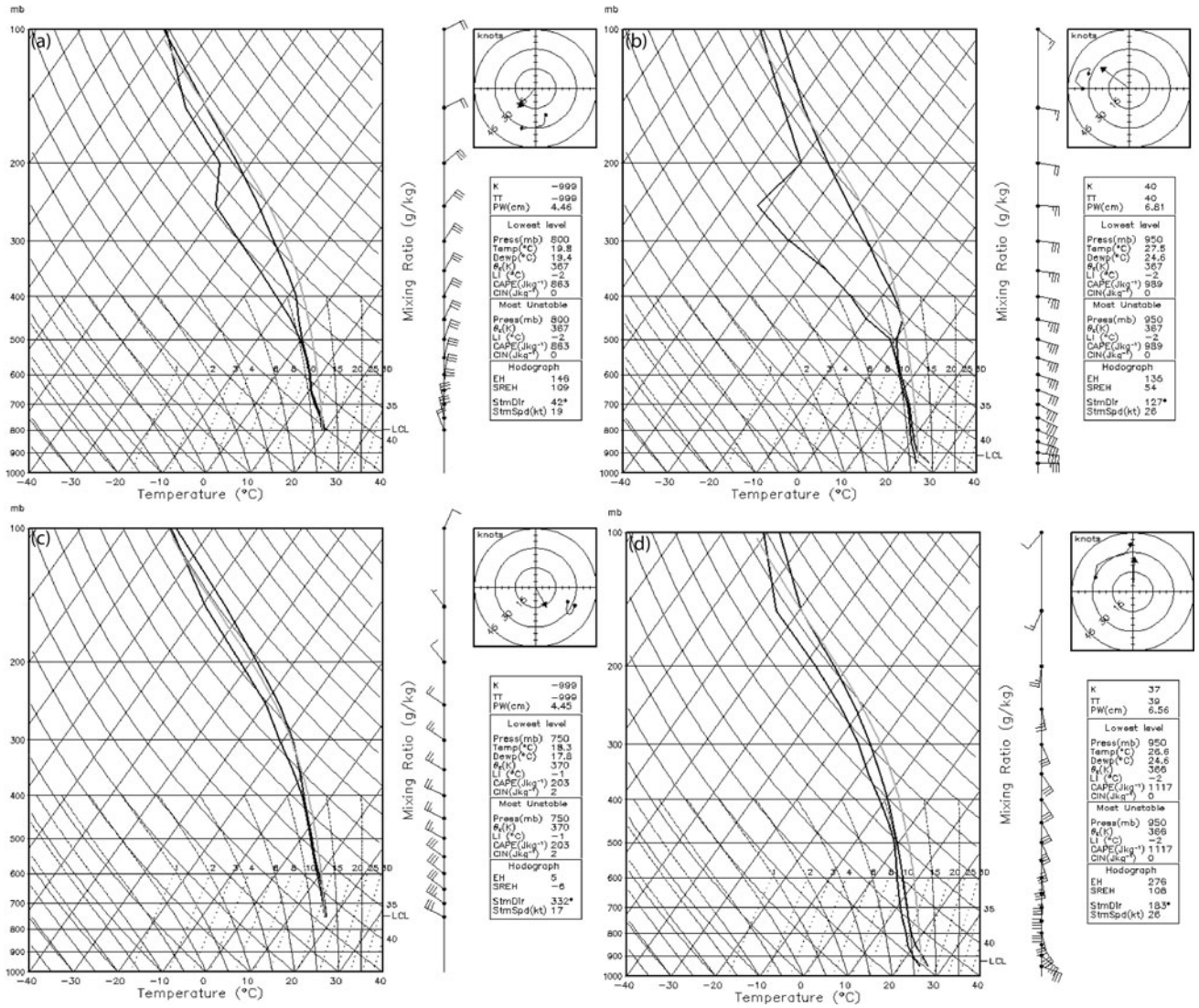

Fig. 15 Skew T diagrams for **a** 0300 UTC 7 August at (23.50°N, 120.76°E) simulated in the CTL-3 case, **b** 0300 UTC 7 August at (23.53°N, 120.59°E) in the NT case, **c** 0000 UTC 8 August at (23.50°N, 120.76°E) simulated in the CTL-3 case, **d** 0300 UTC 8 August at (23.53°N, 120.59°E) in the NT case

most dominant process for generating strong upward motion to produce precipitation.

5.2 The factors of upward motion, water vapor, and translation speed

The total precipitation associated with the passage of a storm can be expressed as (Lin et al. 2001a, b; Lin 2007),

$$P = EwqL_s/c_s, \quad (3)$$

where E is precipitation efficiency, w is vertical velocity, q is specific humidity, L_s is the horizontal scale of the convective system, and c_s is the propagation speed of the convective system (Lin et al. 2001a, b). To make a more rigorous and thorough comparison in this type of ingredient approach, one needs to compare the combined effects of all ingredients, i.e., Eq. (3), versus heavy rainfall amounts for a typhoon before making the comparison of individual terms of Eq. (3). But this study will assume the precipitation efficiency and the horizontal scale of the convective system are constant in the following discussion due to the difficulty in determining them. The major process leading to strong upward motion in producing heavy precipitation connected to Morakot on 8 August is orographic lifting as discussed in Sect. 5a. The daily precipitation on August 7–9 UTC in CTL is 787, 1,925, 457 mm, respectively. The precipitation on August 8 UTC is much larger than that on August 7 and August 9. Hence, it is suitable to apply orographic lifting to the major process leading to strong upward motion in total

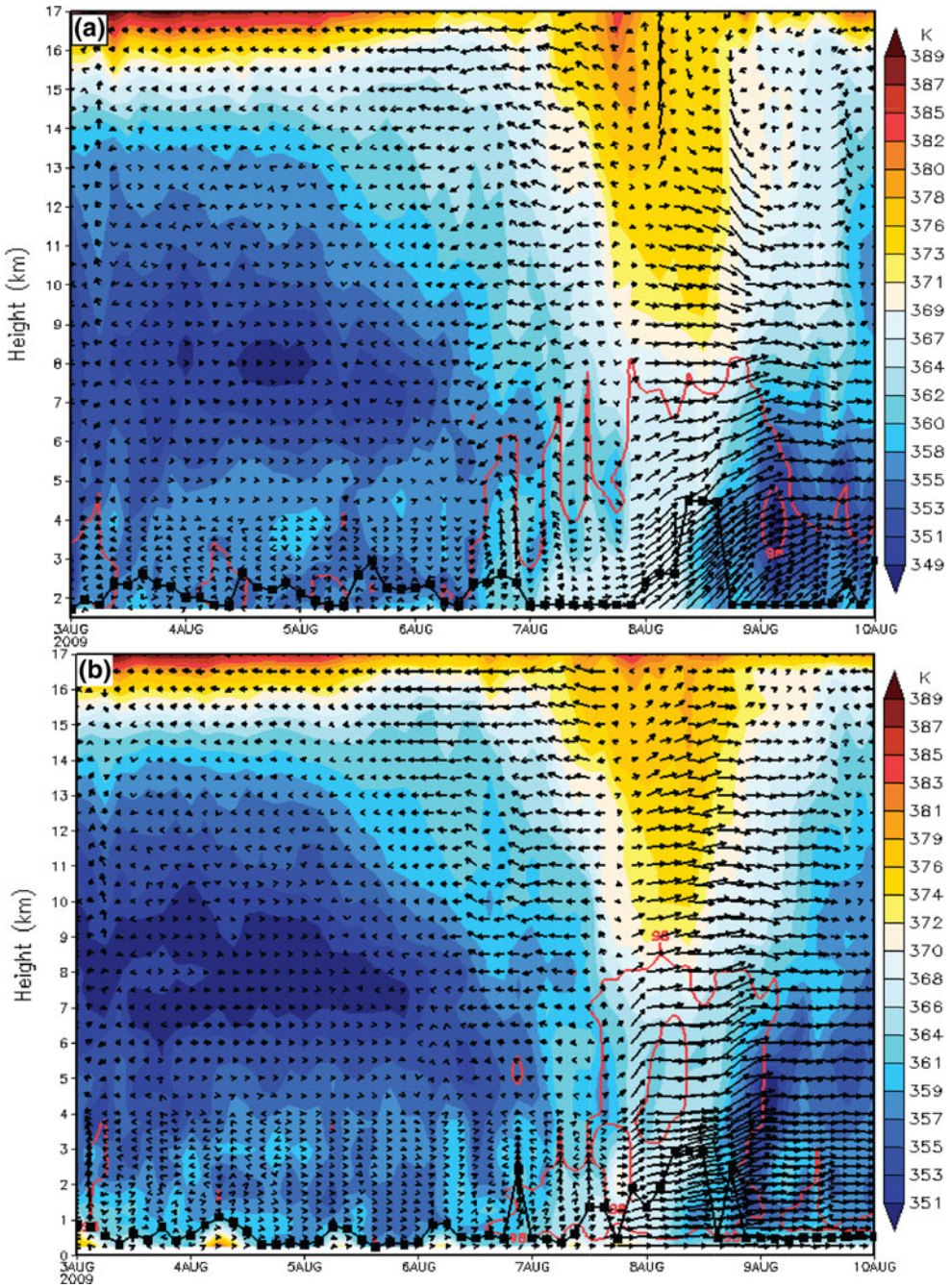

Fig. 16 The time-height cross section of saturated equivalent potential temperature (*shaded*), 98 % relative humidity (*red*), wind vector, and LCL (*black*) simulated in cases of **a** CTL-3 at (23.50°N, 120.76°E) and **b** NT at (23.53°N, 120.59°E)

precipitation. In order to understand the relative importance of orographic lifting, water vapor and the translation speed on the extremely heavy precipitation when Morakot passed by, 11 typhoons, such as Sinlaku (2008), Parma (2009), Jangmi (2008), Fanapi (2010), Nanmadol (2011), Saola (2012), Megi (2010), Krosa (2007), Sepat (2007), Kalmaegi (2008), and Fung-Wong (2008), were chosen to compare with Morakot based on the availability of the storm-relative 16 km microwave-based total precipitable water imagery data and the large maximum accumulated precipitation in a station in Taiwan.

Topography and the track of a typhoon are closely connected to the precipitation pattern of the typhoon. A few differences in the track could lead to very different rainfall patterns. If there are numerous typhoons with a similar track to that of Morakot and with the total precipitable water imagery data, the comparison with Morakot would be easier to carry out. However, because the total precipitable water imagery data employed in this study are only available since 2007, there are not many typhoons that could be compared with Morakot. Every typhoon has its characteristics such as track, lowest sea

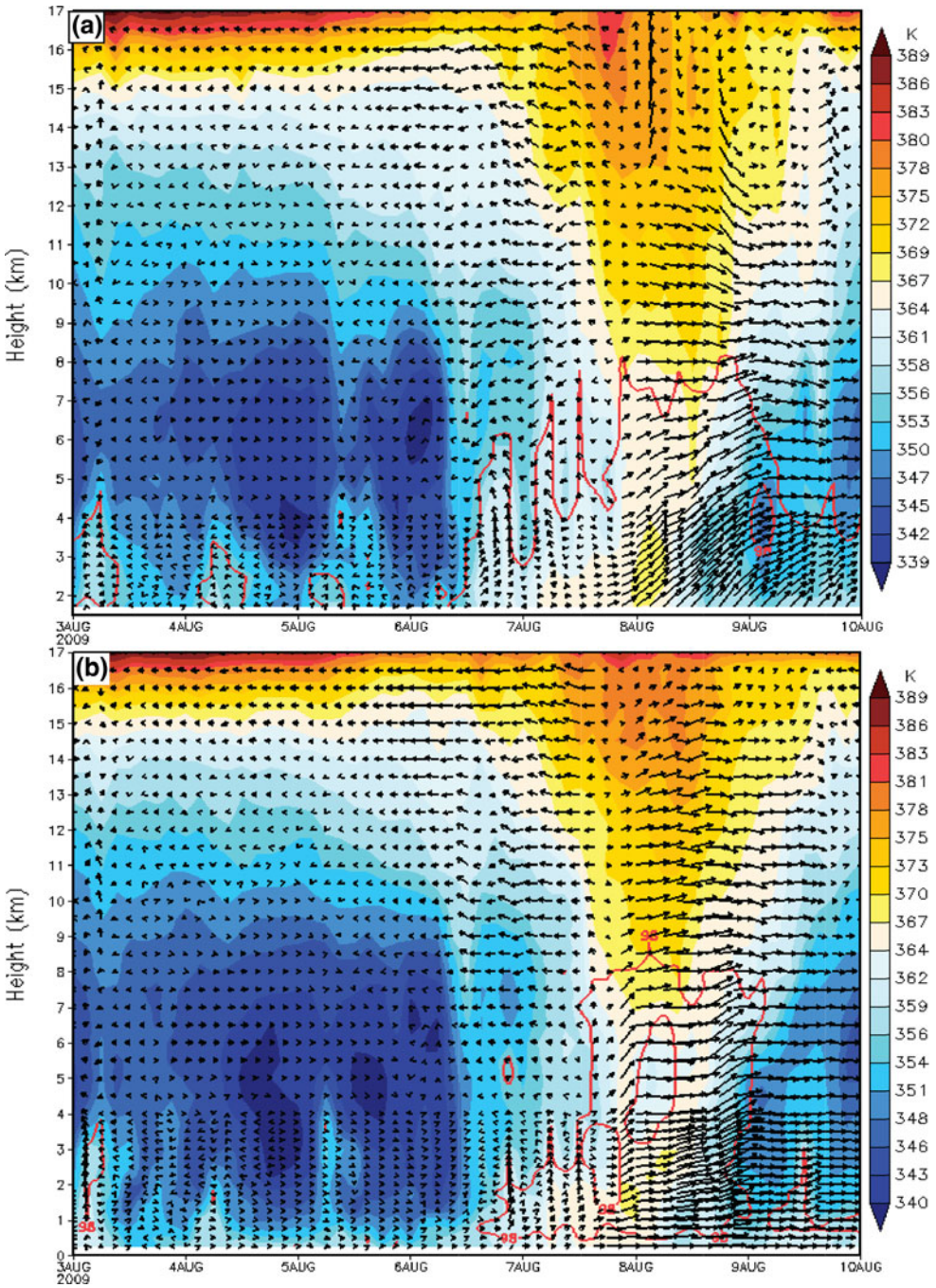

Fig. 17 The time-height cross section of equivalent potential temperature (*shaded*), the 98 % relative humidity (*contours*), and wind vector in cases of **a** CTL-3 at (23.50°N, 120.76°E) and **b** NT at (23.53°N, 120.59°E)

level pressure, rainfall patterns, the large-scale environment, etc. To make the comparison quantitatively, instead of using these characteristics of the typhoons, we consider the most significant impacts on the heavy rainfall in Taiwan, such as the total precipitable water, translation speed, and orographic lifting of Morakot and the 11 typhoons. We will examine which factors made Morakot so unique compared to other 11 typhoons. Generally speaking, if a typhoon's scale is very large, it would produce significant precipitation in Taiwan before making landfall. Hence, the period of slow translation for a typhoon is chosen by its impacts on the rainfall in Taiwan. Our criteria do not require the typhoon under comparison having to make landfall or having a similar track to Morakot. In addition, the calculation of orographic lifting is based on the tangential wind of the typhoon. For cases with typhoon circulation intersecting CMR, we used the maximum wind speed to calculate orographic lifting. For the cases coupled with northeastern monsoon, we use the largest observational local wind speeds near the station with the large accumulated precipitation.

In this study, total precipitable water is used to evaluate the role played by water vapor in the extremely heavy accumulated precipitation. Figure 18 compares the storm relative total precipitable water of Morakot with that of the other 11 typhoons having large maximum accumulated rainfall. Saola (2012) and Morakot have the largest total precipitable water around Taiwan among the 12 typhoons. The large total precipitable water in the case of Saola (2012) lasted for 3 days from 30 July 2012 to 2 August 2012. The abundant water vapor around Taiwan in the case of Morakot has been at least from 6 to 12 August 2009, compared with 4 days, the largest one in the 11 cases. The prevailing southwesterly flow transported abundant water vapor in the vicinity of Taiwan toward CMR when Morakot passed by. Therefore, the excessive water vapor in the case of Morakot produces excessive precipitation than that in the other 11 typhoons given that the other conditions in (3) are comparable such as precipitation efficiency, the horizontal scale of the convective system, upward motion, and translation speed. Hence, the large total precipitable water in a very large region around Taiwan makes abundant water vapor play a significant role in the record-breaking accumulated precipitation.

In addition, the best track data from the web site http://agora.ex.nii.ac.jp/digital-typhoon/index.html.en are used in the translation speeds and maximum wind speed when these typhoons were near Taiwan. Because the track data of the 12 typhoons are from the same data source, the differences in tracks between simulation and different data sources are not an issue. Figure 19 displays the translation speeds when these typhoons were near Taiwan. Among the chosen typhoons, most of them moved no slower than 2.8 ms^{-1} (10 km h^{-1}) as the heavy precipitation associated with these typhoons occurred. Sinlaku (2008) remained slower than 2.5 ms^{-1} from 1200 UTC 12 September to 1200 UTC 14 September except at 1200 UTC 13 September and 0000 UTC 14 September. More than one half of data are not faster than 2.8 ms^{-1} during 13 September–15 September (Fig. 19b). The daily precipitation is at least 200 mm, 800 mm, and 300 mm, respectively, during 13 September–15 September at the station with the largest accumulated rainfall connected with Sinlaku (2008). Thus, the large accumulated precipitation (1,617 mm) is closely related to the slow translation when Sinlaku (2008) moved close to Taiwan, especially its total precipitable water is next to the least in the 12 typhoons (Fig. 18b). Parma (2009) moved slower than 2 ms^{-1} during 0600 UTC 4 October–1200 UTC 5 October (Fig. 19c). As Parma's slow translation, the northward-moving rainbands led to 1519 mm accumulated precipitation in Yilan County. The rainbands propagated northward from the Bashi Channel to northeastern Taiwan one after another. Without the slow translation, the pattern of accumulated precipitation associated with Parma (2009) will change dramatically and thus large accumulated precipitation accordingly. Except 0600 UTC 28 August and 1800 UTC 28 August, Nanmadol (2011) propagated slower than or equal to 2.8 ms^{-1} from 0000 UTC 28 August to 1800 UTC 30 August (Fig. 19f). The slow translation resulted in at least 200, 200, and 300 mm on 28 August, 29 August, and 30 August, respectively, at the station with the largest accumulated rainfall (1,080 mm) associated with Nanmadol (2011). Megi (2010) remained no faster than 2.3 ms^{-1} during 0000 UTC 21 October–1800 UTC 21 October (Fig. 19h). About two-third of the largest accumulated precipitation (1195 mm) associated with Megi (2010) happened during the period of slow translation 0000 UTC 21 October–1800 UTC 21 October (Fig. 21a). Therefore, slow translation speed is the crucial factor of the large accumulated precipitation with the help of abundant water vapor (Figs. 18h, 19h, 21a). Hence, slow translation does have great effects on the large accumulated precipitation of Sinlaku (2008), Parma (2009), Nanmadol (2011), and Megi (2010).

However, the slow movement of Morakot is only in 0600 UTC 7 August and during 0000 UTC 8 August–1200 UTC 8 August (Fig. 19a). The slow movement during the period caused more precipitation than a fast moving typhoon does according to (3). But the slow moving speed of 1.1–1.5 ms^{-1} during 0000 UTC 8 August–1200 UTC 8 August is not slower than 0.5 ms^{-1} in Sinlaku (2008), 0.7 ms^{-1} in Parma (2009) and Nanmadol (2011) (Fig. 19). The duration of slow moving speed of Morakot is much shorter than that in Sinlaku (2008), Parma (2009), Nanmadol (2011) and Megi (2010). Thus, the slow movement of Morakot during 0000 UTC 8 August–1200 UTC 8 August does not outrank that in Sinlaku (2008), Parma (2009), Nanmadol (2011) and Megi (2010).

Furthermore, the precipitation around 0600 UTC 7 August is not important at the Alishan station with the maximum accumulated rainfall associated with Morakot (Fig. 21b). Only about 22 % (640 mm) of the largest accumulated precipitation (2,855 mm) associated with Morakot did happen during the period of slow translation 0000 UTC 8 August–1200 UTC 8 August (Fig. 21b). Without the 640 mm rainfall during 0000 UTC 8 August–1200 UTC 8 August, still the accumulated precipitation allied with Morakot is much larger than that in the other 11 typhoons. The hourly precipitation during 0000 UTC 8 August–1200 UTC 8 August cannot be ranked top seven of the Alishan station associated with Morakot (Fig. 21b). Relatively, the slow translation of Sinlaku (2008), Parma (2009), Nanmadol (2011) and Megi (2010) did have large

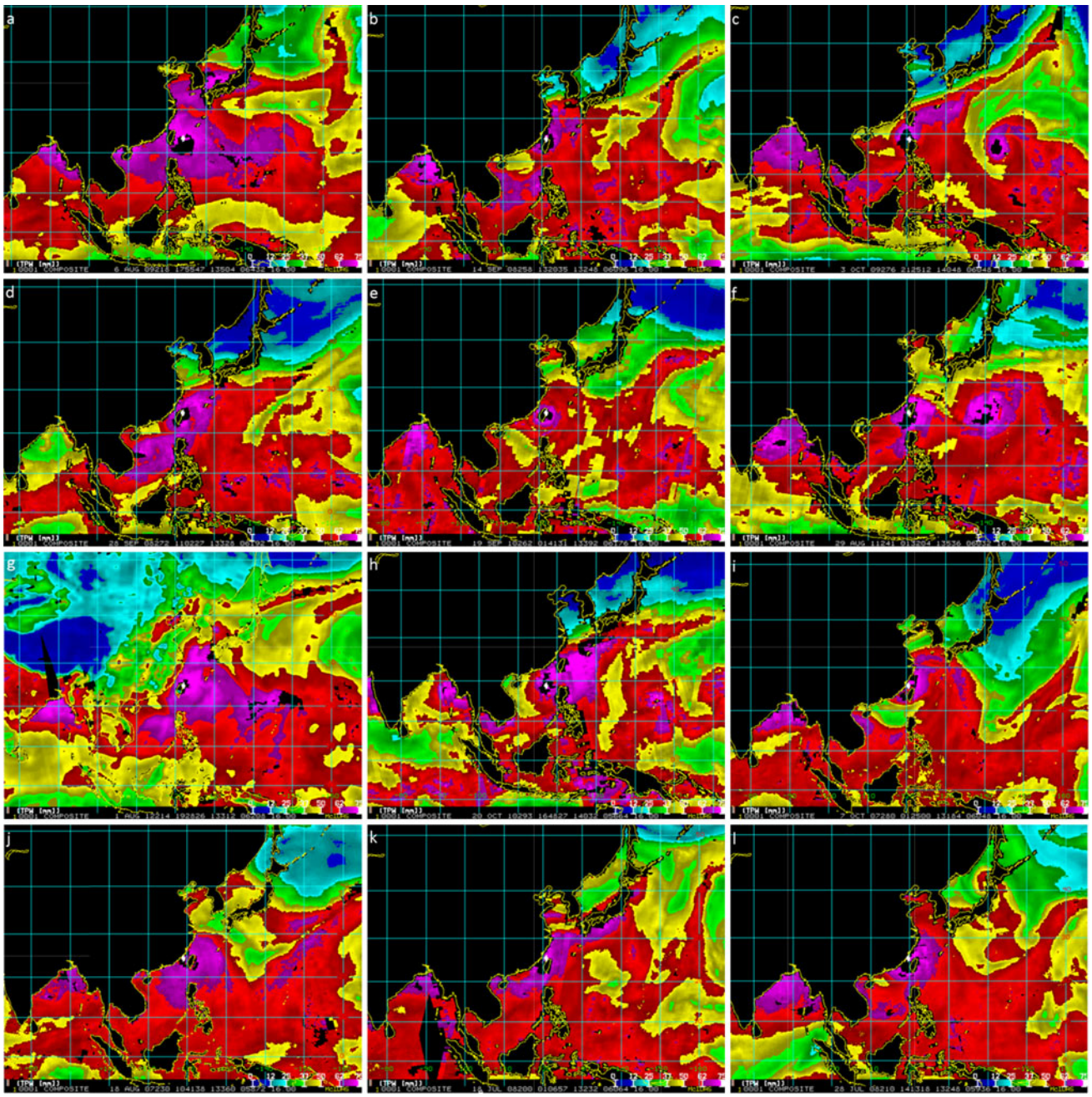

Fig. 18 The storm relative 16 km microwave-based total precipitable water imagery on **a** 1755 UTC 6 August 2009 around Typhoon Morakot (2009), **b** 1320 UTC 14 September 2008 around Typhoon Sinlaku (2008), **c** 0745 UTC 4 October 2009 around Typhoon Parma (2009), **d** 1245 UTC 28 September 2008 around Typhoon Jangmi (2008), **e** 0141 UTC 19 September 2010 around Typhoon Fanapi (2010), **f** 1346 UTC 28 August 2011 around Typhoon Nanmadol (2011) **g** 1928 UTC 1 August 2012 around Typhoon Saola (2012), **h** 1648 UTC 20 Oct around Typhoon Megi (2010), **i** 0125 UTC 7 October around Typhoon Krosa (2007), **j** 1041 UTC 18 August around Typhoon Sepat (2007), **k** 0106 UTC 18 July around Typhoon Kalmaegi (2008), and **l** 1413 UTC 28 July around Typhoon Fung-Wong (2008)

influences on its large accumulated precipitation, whereas the slow translation do not appear so critical for Morakot. The impacts of slow translation should not be over-emphasized on the record-breaking accumulated precipitation associated with Morakot. Therefore, we conclude that the slow translation speed is not the most important process bringing about the extremely heavy precipitation which is much larger than that in these 11 typhoons, but rather only a factor resulting in the extremely heavy rainfall.

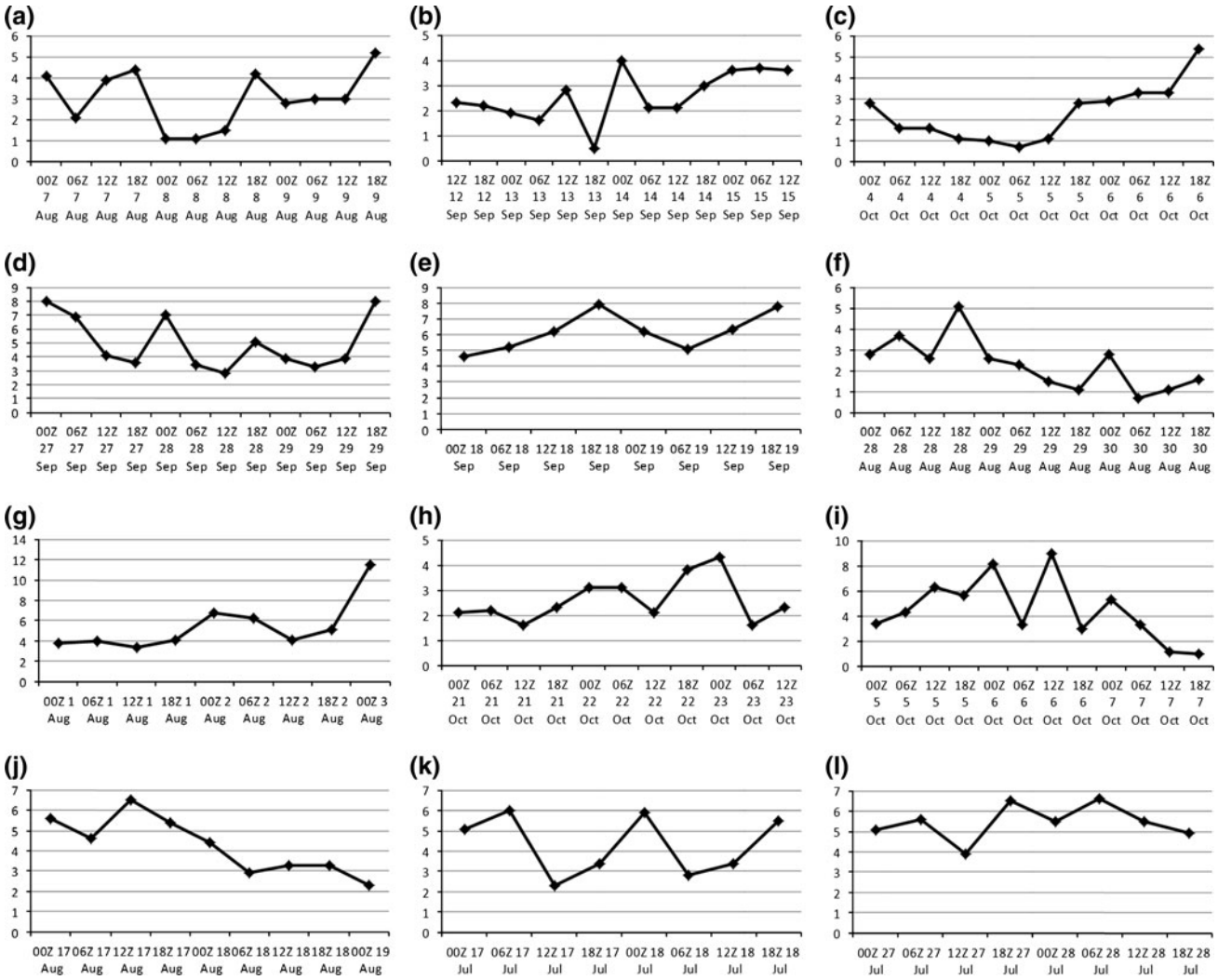

Fig. 19 The moving speeds (ms^{-1}) every 6 h for Typhoon **a** Morakot (2009), **b** Sinlaku (2008), **c** Parma (2009), **d** Jangmi (2008), **e** Fanapi (2010), **f** Nanmadol (2011), **g** Saola (2012), **h** Megi (2010), **i** Krosa (2007), **j** Sepat (2007), **k** Kalmaegi (2008), and **l** Fung-Wong (2008)

Orographic-induced vertical velocity can be calculated by the following equation (Lin et al. 2001a, b; Lin 2007).

$$w_{\text{oro}} = U\frac{\partial h}{\partial x} \tag{4}$$

The maximum wind speeds in these 12 typhoons are illustrated in Fig. 20. The orographic lifting of several typhoons making landfall in Taiwan with large wind speeds is calculated in Table 2. The maximum wind speed of Morakot when it generated extremely heavy precipitation was about 31.3 ms^{-1}, which is much smaller than 35.0 ms^{-1} in Sinlaku (2008), 57.3 ms^{-1} in Jangmi (2008), 37.0 ms^{-1} in Fanapi (2010), 33.3 ms^{-1} in Saola (2012), 40.3 ms^{-1} in Krosa (2007), and 37.5 ms^{-1} in Fung-Wong (2008). The locations with maximum accumulated precipitations of these typhoons are all in the mountainous regions. Actually, the slope of terrain depends on the direction. In the study, the slope of terrain is calculated by the slope from the city in plain according to the direction of typhoon translation. The orographic lifting of Morakot is the sixth in the typhoons on Table 2 because Morakot is category 1 typhoon with much weaker wind speed than other typhoons. Especially, the orographic lifting of Jangmi (2008), Krosa (2007), Fanapi (2010), and Sinlaku (2008) is much larger than that of Morakot. Hence, the orographic lifting of Morakot is not the most important process to generate much more precipitation than that in Jangmi (2008), Krosa (2007), Fanapi (2010), and Sinlaku (2008), but rather only a factor resulting in the extremely heavy rainfall.

From the above discussion, we found that both Morakot and Saola (2012) have much more total precipitable water than that of the other typhoons; that Parma (2009), Nanmadol (2011), Megi (2010), and Sinlaku (2008) have

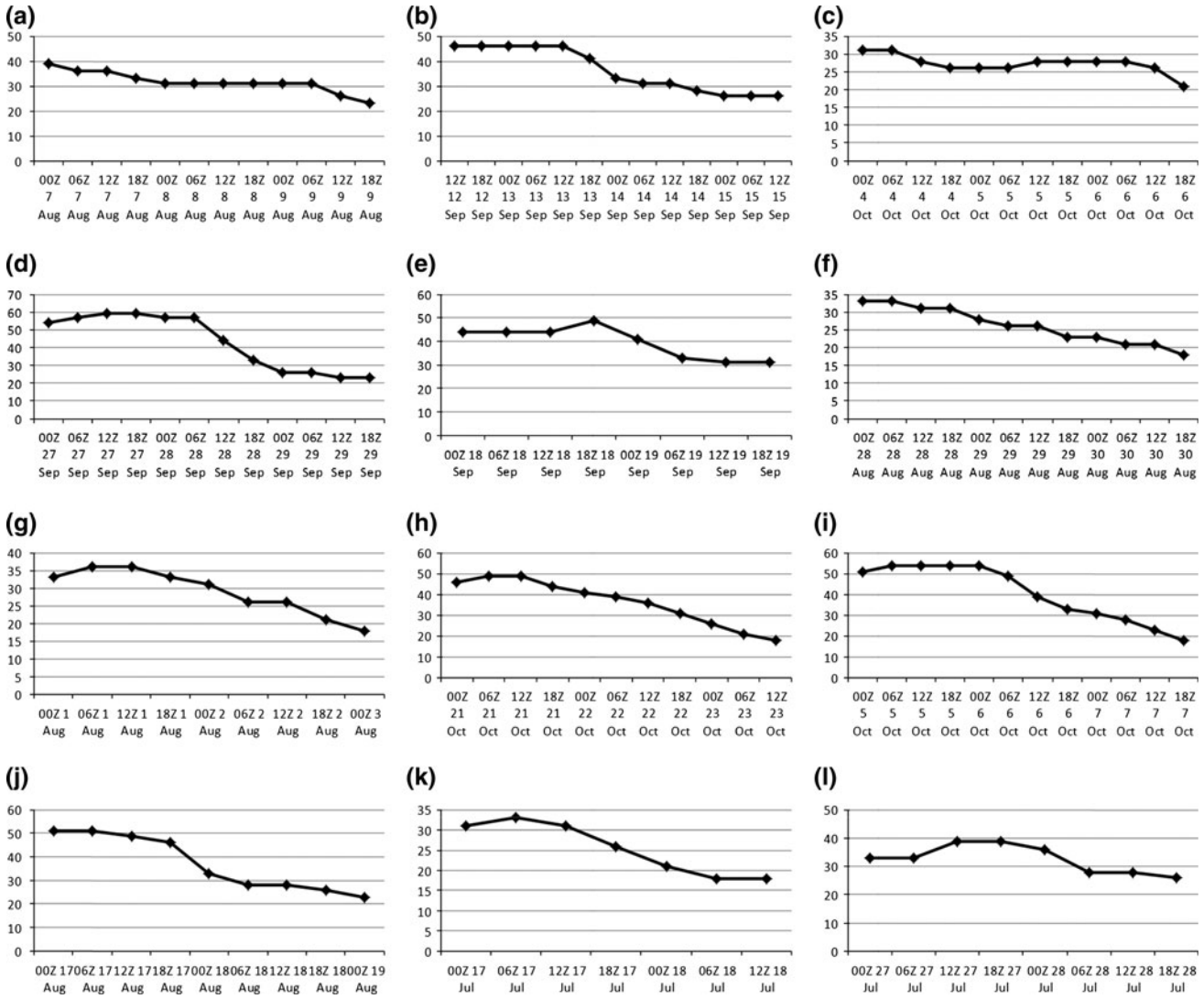

Fig. 20 The maximum wind speeds (ms^{-1}) every 6 h for Typhoon **a** Morakot (2009), **b** Sinlaku (2008), **c** Parma (2009), **d** Jangmi (2008), **e** Fanapi (2010), **f** Nanmadol (2011), **g** Saola (2012), **h** Megi (2010), **i** Krosa (2007), **j** Sepat (2007), **k** Kalmaegi (2008), and **l** Fung-Wong (2008)

much slower translation than that of the other typhoons; and that Jangmi (2008), Krosa (2007), Fanapi (2010), and Sinlaku (2008) have much larger orographic lifting than that of the other typhoons. It may well to characterize the above nine typhoons as total precipitable water, slow translation, or orographic lifting accordingly. Sinlaku (2008) is characterized by both slow translation and orographic lifting, which is probably why its maximum accumulated precipitation is the third among 12 typhoons when its total precipitable water is next to the least (Tables 2, 3; Fig. 18b). The maximum accumulated rainfalls associated with these nine typhoons are the top nine accumulated precipitation among the 12 typhoons in this study (Table 3). As all of the total precipitable water, slow translation, and orographic lifting are at most ordinary among the 12 typhoons, the maximum accumulated rainfalls of Sepat (2007), Kalmaegi (2008) and Fung-Wong (2008) are less than that of the above nine typhoons. The maximum accumulated precipitation associated with Morakot and Saola (2012) is the top two ones among the 12 typhoons. This implies that total precipitable water could be more important than slow translation and orographic lifting in maximum accumulated precipitation, because total precipitable water could help to increase the rain rate in calculating precipitation efficiency. The much larger maximum accumulated precipitation connected with Morakot than that connected with Saola (2012) is due to much slower translation [3 ms^{-1} of Morakot versus 5.4 ms^{-1} of Saola (2012) on average in the periods in Fig. 19a, g] and larger orographic lifting [2.74 ms^{-1} in Morakot versus 2.58 ms^{-1} in Saola (2012) in Table 2] associated with Morakot.

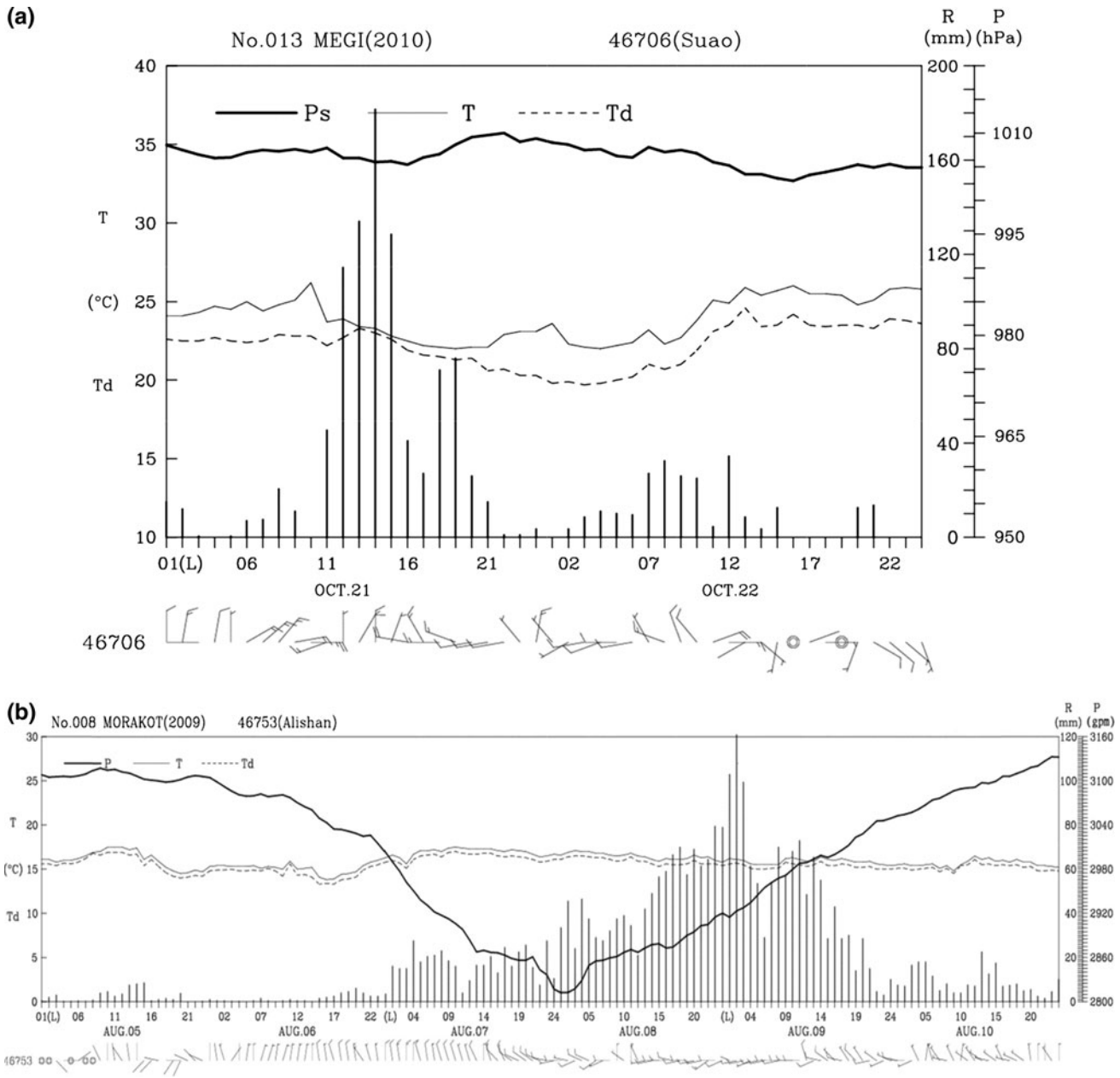

Fig. 21 The hourly precipitation, station pressure, temperature, dew point temperature influenced by Typhoon **a** Megi (2010) at Suao and **b** Morakot (2009) at Alishan

It is clear from Eq. (3) that all of the upward motion, water vapor and translation speed of a storm directly contribute to the total rainfall. After the quantitative comparison of total precipitable water vapor, translation speed, and orographic lifting between Morakot and these 11 typhoons, the translation speed and orographic lifting of Morakot do not outrank those of all these 11 typhoons with large maximum accumulated precipitation. And thus, the translation speed and orographic lifting cannot shed light on much more maximum accumulated rainfall associated with Morakot than that associated with these 11 typhoons. In contrast, the total precipitable water vapor around Taiwan in the Morakot case is much more than that in these 11 typhoons except Saola (2012) and last much longer than these 11 typhoons. Therefore, in terms of the much larger maximum accumulated precipitation associated with the passage of Morakot than that in these 11 typhoons, the abundant water vapor around Taiwan overshadows the slow translation and orographic lifting.

Table 2 Comparison of orographic lifting associated with several typhoons passing over Taiwan's CMR

Typhoon	Station	Station height (m)	City height (m)	Distance (m)	Slope*	U* (ms^{-1})	Orographic lifting (ms^{-1})
Morakot	46753	2,413	120	26,154	0.0877	31.3	2.74
Sinlaku	C1F94	2,605	234	25,577	0.0927	35.0	3.24
Jangmi	C0U71	1,950	60	24,359	0.0776	57.3	4.45
Fanapi	C1R14	1,166	300	9,744	0.0889	37.0	3.29
Saola	C0U71	1,950	60	24,359	0.0776	33.3	2.58
Krosa	C0M53	1,405	120	14,871	0.0864	40.3	3.48
Sepat	C1R14	1,166	300	9,744	0.0889	30.5	2.71
Fung-Wong	C0U71	1,950	60	24,359	0.0776	37.5	2.91

* The terrain slope is calculated by the slope from the city in plain to the station according to the direction of typhoon translation. The wind speed is the mean wind speed when the typhoon is around Taiwan

Table 3 Accumulated precipitation associated with the typhoons in the analysis

Typhoons	Accumulated rainfall (mm)
Morakot (2009)	2,855
Saola (2012)	1,786
Sinlaku (2008)	1,617
Parma (2009)	1,519
Megi (2010)	1,195
Jangmi (2008)	1,135
Fanapi (2010)	1,127
Krosa (2007)	1,118
Nanmadol (2011)	1,080
Sepat (2007)	987
Kalmaegi (2008)	963
Fung-Wong (2008)	830

6 Summary

In this study, the storm relative 16 km microwave-based total precipitable water imagery is used to examine the role of water vapor availability played on the extremely heavy rainfall associated with the passage of Typhoon Morakot (2009) over Taiwan's Central Mountain Range (CMR). The WRF-ARW model is employed to conduct numerical simulations to investigate the time evolution of three-dimensional structure, and the factors causing the extremely heavy precipitation on the precipitation connected to Morakot. The control case (CTL) successfully reproduces the track, the track deflection, characteristic of rainbands, and precipitation patterns and maxima compared with best track analysis, maximum radar reflectivity, and rain gauge. Especially the location of maximum accumulated rainfall in the CTL with grid interval 3 km is only <5.7 km away from observations.

We found that the diameter of eye is larger than 0.78° width in latitude at 23.5°N at 1200 UTC 7 August in the strongest stage. The cloud-free eye has contracted much smaller after landfall, and then disappeared within 2 h afterward. The high-level anticyclonic outflow of the secondary circulation near the eyewall is not very clear even during the strongest stage. During the landfall, the deep convection on the west (windward) side of the CMR in the CTL helps strengthen the secondary circulation over the land. Similarly, the deep convection over the land helps forming the secondary circulation in the experiment without terrain. Within 5 h after landfall in the CTL, deep convection, secondary circulation and vertical tilt of maximum wind all disappear, and the eyewall collapses that is closely associated with limited precipitation along the track after landfall. Due to the lack of high and steep CMR in the case NT, the eyewall decay is slower than that in the CTL case. With the extra water vapor, latent heat, and sensible heat in the case of OC, the storm develops continuously after passing over Taiwan, and thus, the secondary circulation is much clearer than that during the ocean stage in the CTL case.

It is shown in the CTL case that the larger wind speed, convergence, upward motion, and relative humidity close to the Morakot's center are limited when it passes northern Taiwan, whereas they are located to the south away from Morakot's center. Due to the interactions between Morakot's circulation, the high and steep CMR, and the prevailing southwesterly flow, the major precipitation associated with the passage of Morakot is located to the south and away from the Morakot's center. Hence, there is no deep convection close to Morakot's center when it crossed northern Taiwan, and thus the precipitation is limited. Therefore, the asymmetric precipitation pattern is pretty obvious. The processes which might produce strong upward motion leading to extremely heavy precipitation during 0000 UTC 8 August–0000 UTC 9 August are

initiated by orographic lifting, especially compared to the upstream convergence. Nevertheless, before 0000 UTC 8 August, these instabilities cannot be ignored to be responsible for the precipitation.

A quantitative comparison of total precipitable water, translation speed, and orographic lifting with those of 11 typhoons in recent years bringing extremely heavy precipitation to Taiwan, Morakot possesses much more abundant water vapor around Taiwan except Saola (2012). The abundant water vapor in the case of Morakot lasts much longer than these 11 typhoons. Morakot does not move more slowly than the four slow typhoons do. The duration of slow translation in the Morakot case is much shorter than the slow moving typhoons. The maximum wind speed of Morakot is much smaller than that in six typhoons with large wind speed, and thus the calculated orographic lifting in Morakot is smaller than that in the five typhoons with large wind speed. Therefore, considering the factors leading to the extremely heavy rainfall associated with Morakot, we found that the abundant water vapor outweighs slow translation speed and orographic lifting. The slow translation speed and orographic lifting are two minor factors helping to generate the extremely heavy rainfall.

Note that two typhoons, Morakot and Saola (2012), both of them contain the largest total precipitable water and maximum accumulated precipitation among these 12 typhoons, show strong impacts of large total precipitable water on maximum accumulated precipitation. This could be due to the relationship between total precipitable water and precipitation efficiency and need further study to clarify it.

Acknowledgments The authors would like to thank Prof. C.-S. Chen for discussions, and acknowledge the reviewers for their very helpful comments. This research was supported by the NOAA Educational Partnership Program (EPP) under Cooperative Agreement No: NA06OAR4810187.

References

Bender MA, Tuleya RE, Kurihara Y (1987) A numerical study of the effect of island terrain on tropical cyclones. Mon Wea Rev 115:130–155. doi:10.1175/1520-0493(1987)115<0130:ANSOTE>2.0.CO;2

Chan J, Gray W (1982) Tropical cyclone movement and surrounding flow relationships. Mon Wea Rev 110:1354–1374

Chen Y, Yau MK (2003) Asymmetric structures in a simulated landfalling hurricane. J Atmos Sci 60:2294–2312. doi:10.1175/1520-0469(2003)060<2294:ASIASL>2.0.CO;2

Chien F-C, Kuo H-C (2011) On the extreme rainfall of Typhoon Morakot (2009). J Geophys Res 116:D05104. doi:10.1029/2010JD015092

Cressman GP (1959) An operational objective analysis system. Mon Wea Rev 87:367–374

Doswell CA III, Brooks H, Maddox R (1996) Flash flood forecasting: an ingredient-based methodology. Wea Forecasting 11:560–581

Dudhia J (1989) Numerical study of convection observed during the winter monsoon experiment using a mesoscale two-dimensional model. J Atmos Sci 46:3077–3107

Ge X, Li T, Zhang S, Peng M (2010) What causes the extremely heavy rainfall in Taiwan during Typhoon Morakot (2009)? Atmos Sci Lett 11:46–50

Hong S-Y, Noh Y, Dudhia J (2006) A new vertical diffusion package with an explicit treatment of entrainment processes. Mon Wea Rev 134:2318–2341

Hong C–C, Lee M-Y, Hsu H–H, Kuo J-L (2010) Role of submonthly disturbance and 40–50 day ISO on the extreme rainfall event associated with Typhoon Morakot (2009) in Southern Taiwan. Geophys Res Lett 37:L08805. doi:10.1029/2010GL042761

Huang C-Y, Wong C-S, Yeh T-C (2011) Extreme rainfall processes exhibited by Typhoon Morakot (2009). Terr Atmos Ocean Sci 22:613–632

Jou BJ-D, Yu Y-C, Lei F, Chen Y-M, Lee C-S, Cheng M-D (2010) Synoptic environment and rainfall characteristics of Typhoon Morakot (0908). Atmos Sci 38:21–38 (in Chinese)

Kain JS (2004) The Kain–Fritsch convective parameterization: an update. J Appl Meteor 43:170–181

Kidder SQ, Jones AS (2007) A blended satellite total precipitable water product for operational forecasting. J Atmos Oceanic Technol 24:74–81

Lee W-C, Jou BJ-D, Chang P-L, Marks FD (2000) Tropical cyclone kinematic structure retrieved from single-Doppler radar observations. Part III: evolution and structures of Typhoon Alex (1987). Mon Wea Rev 128(12):3982–4001

Liang J, Wu L, Ge X, Wu C–C (2011) Monsoonal Influence on Typhoon Morakot (2009) Part II: numerical Study. J Atmos Sci 68:2222–2235

Lin Y-L (2007) Mesoscale Dynamics. Cambridge University Press, Cambridge

Lin Y-L, Chiao S, Wang T-A, Kaplan ML (2001a) Some common ingredients for heavy orographic rainfall. Weather Forecast 16:633–660

Lin Y-L, Chiao S, Wang TA, Kaplan ML, Weglarz RP (2001b) Some common ingredients for heavy orographic rainfall. Weather Forcast 16:633–660

Lin C-Y, Hsu H-M, Sheng Y-F, Kuo C-H, Liou Y-A (2011) Mesoscale processes for super heavy rainfall of Typhoon Morakot (2009) over Southern Taiwan. Atmos Chem Phys 11:345–361. doi:10.5194/acp-11-345-2011

Mlawer EJ, Taubman SJ, Brown PD, Iacono MJ, Clough SA (1997) Radiative transfer for inhomogeneous atmospheres: RRTM, a validated correlated-k model for the longwave. J Geophys Res 102:16,663–16682

Nguyen HV, Chen Y-L (2011) High resolution initialization and simulations of Typhoon Morakot (2009). Mon Wea Rev 139:1463–1491

Reisner J, Rasmussen RM, Bruintjes RT (1998) Explicit forecasting of supercooled liquid water in winter storms using the MM5 forecast model. Q J Roy Meteor Soc 124:1071–1107

Simpson RH (1974) The hurricane disaster-potential scale. Weatherwise 27:169–186

Skamarock WC, Klemp JB, Dudhia J, Gill DO, Barker DM, Duda M, Huang X-Y, Wang W, Powers JG (2008) A Description of the Advanced Research WRF Version 3. NCAR Technical Note, NCAR/TN-475 + STR

Smith RB (1979) The influence of mountains on the atmosphere. Adv Geophys 21:87–230

Tao W-K, Simpson J, McCumber M (1989) An ice-water saturation adjustment. Mon Weather Rev 117:231–235

Thompson G, Rasmussen RM, Manning KW (2004) Explicit forecasts of winter precipitation using an improved bulk microphysics scheme. Part I: description and sensitivity analysis. Mon Weather Rev 132:519–542

Tuleya RE (1994) Tropical storm development and decay: sensitivity to surface boundary conditions. Mon Weather Rev 122:291–304. doi:10.1175/1520-0493(1994)122<0291:TSDADS>2.0.CO;2

Wang TCC, Tang Y-S, Wei C-H, Lin P-L, Liou Y-C, Chang W-Y, Chou C-B, Ji B-T, Lin C-Y (2010) The precipitation characteristics of Typhoon Morakot (2009) from radar analyses. Atmos Sci 38:39–61 (in Chinese)

Wu C–C, Huang C-Y, Yang M-J, Chien F-C, Hong J-S, Yen T-H (2010) Typhoon Morakot (2009) and a special review on the current status and future challenge of tropical cyclone simulation (in Chinese). Atmos Sci 38:99–134

Wu L, Liang J, Wu C–C (2011) Monsoonal influence on Typhoon Morakot (2009) Part I: observational analysis. J Atmos Sci 68:2208–2221

Xu X, Lu C, Xu H, Chen L (2011) A possible process responsible for exceptional rainfall over Taiwan from Typhoon Morakot. Atmos Sci Leti 12:294–299

Yang M-J, Zhang D-L, Tang X-D, Zhang Y (2011) A modeling study of Typhoon Nari (2001) at landfall: 2. Structural changes and terrain-induced asymmetries. J Geophys Res 116:D09112. doi:10.1029/2010JD015445

Yen T-H, Wu C–C, Lien G-Y (2011) Rainfall simulations of Typhoon Morakot with controlled translation speed based on EnKF data assimilation. Terr Atmos Ocean 22:647–660. doi:10.3319/TAO.2011.07.05.01(TM